Journal of Sound and Vibration (1998) **211**(5), 877–906

EXTENSIONS OF THE PHASE SPACE LINEARIZATION (PSL) TECHNIQUE FOR NON-LINEAR OSCILLATORS

R. N. IYENGAR

Central Building Research Institute, *Roorkee* 247667, *India*

D. ROY

Engineering Mech. Research Corp., 907 *Barton Centre*, 84, *M.G. Road*, *Bangalore* 560 001, *India*

(*Received* 17 *May* 1996, *and in final form* 10 *November* 1997)

This paper is devoted to further exploration of the PSL technique developed earlier in its companion paper. To start with, it is shown that the method is not only appicable for obtaining one-periodic orbits, but can be made use of for obtaining every conceivable orbit, including subharmonic or period-doubled orbits, quasi-periodic orbits and even chaotic orbits. This is numerically illustrated by constructing various such orbits of Ueda's, Duffing-Holmes' and Van der Pol's oscillators. Next, the separatrix, that separates the basins of attraction of the stable limit cycles of Duffing-Holmes' oscillator, is constructed using the PSL procedure. A possibility of predicting the chaotic diffusion of trajectories based on a heuristic argument of a near-tangency of stable and unstable limit cycles of Duffing-Holmes' oscillator is also discussed. Finally, the PSL scheme is made use of to compute various characteristic quantities such as Fourier spectra, Liapunov characteristic exponents and probability density functions. Many new results are presented to establish the versatility of the PSL method.

1. INTRODUCTION

In the companion paper [1], a novel piecewise linearization technique for non-linear oscillators was introduced. It was shown that the technique may be used for the dual purpose of numerically integrating the non-linear ODE and extracting a rich spectrum of information about the local flow structure near any point in the phase space, which need not be a hyperbolic fixed point. However, the scheme was numerically verified only against the free vibration response and a few forced vibration one-periodic responses of a class of non-linear oscillators. It is well known that many of the non-linear oscillators under harmonic excitations may give rise to a wide variety of response characteristics, such as subharmonic periodicity, quasi-periodicity and even chaos. Even though the existing numerical techniques such as the Runge-Kutta method have been extensively used in the literature to obtain time histories or phase space representations of all such orbits, the selection of a proper time step, Δt, for convergence to the exact solution remains an unresolved issue [2]. Depending upon the time-step, fictitious incidences such as occurrence of a *computational chaos* [3] or *shadowing of a chaotic orbit* [4, 5] may take place. Several efforts to study the Poincaré section or the solution trajectories using the Taylor series expansions have been made [6, 7]. However, these methods require extensive computations and are rather unwieldy even with the use of such computer-algebra softwares as

0022–460X/98/150877 + 30 $25.00/0/sv971430

MACSYMA, *MATHEMATICA*, *MAPLE* or *REDUCE*. Another problem that has received attention in the literature is prediction of the behaviour of the forced separatrix in double well potential oscillators, such as the Duffing-Holmes oscillator [8]. For the Duffing-Holmes oscillator, the forced separatrix may be considered to be the boundary that separates the basins of attraction of the two stable limit cycles. The forced separatrix may be considered to be the stable manifold of the saddle type (unstable) periodic orbit surrounding the origin. Moreover, an unstable manifold of this periodic orbit also exists. It is the transversal homoclinic intersection of these stable and unstable manifolds that leads to a complicated dynamical behaviour, such as the Smale horseshoe. An accurate determination of these manifolds is however not possible by conventional schemes of numerical integration.

With this in view, the present paper is so organized as to partially answer some of these questions using the PSL method. In particular, an attempt is made to simulate the subharmonic, quasi-periodic and chaotic response of several second order non-linear systems, namely Duffing-Holmes', Ueda's and Van der Pol's oscillators. This is followed by an exploration of the possibility of constructing the stable and unstable manifolds of the unstable periodic orbit of the Duffing-Holmes oscillator. It is known that the destruction of the double well potential structure in the phase plane precedes a chaotic diffusion of trajectories for this oscillator. An attempt is made to predict such a diffusion in the parameter space by computing the near-tangency of the stable and unstable limit cycles, obtained via the linearization procedure. Finally, it is shown that several characteristic quantities, such as Liapunov characteristic exponents, Fourier spectra and probability density functions, can also be computed accurately by suitably exploiting the concept of phase space linearization.

2. COMPLICATED RESPONSES

It was shown in the companion paper [1] that using the concept of equivalent linearization over sufficiently small segments of orbits in the relevant phase space, it is possible to reduce a non-linear oscillator of the form

$$\ddot{x} + c\dot{x} + kx + \xi(x, \dot{x}) = F\cos(\lambda t), \qquad x \in \mathbf{R}^1, \tag{1}$$

to the equivalent linear form

$$\ddot{x} + \eta(x_i, \dot{x}_i)\dot{x} + \beta(x_i, \dot{x}_i)x = F\cos(\lambda t). \tag{2}$$

Here it may be recalled that the above ODE which is conditionally linear given the dependent variables $\{x_i, \dot{x}_i\}$ at the time instant t_i, is valid only over a small segement $[\{x_i, \dot{x}_i\}, \{x_{i+1}, \dot{x}_{i+1}\}]$ in the phase plane. Now it would be interesting to take a closer look at the linear equation (2). From the complementary function associated with this equation, the following pair of eigenvalues can readily be extracted

$${}^i\lambda_{1,2} = -0{\cdot}5\eta(x_i, \dot{x}_i) \pm 0{\cdot}5\sqrt{\sigma}, \tag{3}$$

where

$$\sigma = \eta^2(x_i, \dot{x}_i) - 4\beta(x_i, \dot{x}_i). \tag{4}$$

If ${}^i\lambda_{1,2}$ are complex conjugates with negative real parts, then the corresponding local solution would be stable. Moreover, for complex conjugate eigenvalues with negative real parts, the local solutions are asymptotically periodic. On the other hand, if ${}^i\lambda_{1,2}$ are both real with at least one of them being positive, or complex conjugates with positive real parts, then the corresponding orbits are saddle type of non-periodic orbits. It may be observed

that the values of the real parts of the eigenvalues ${}^{i}\lambda_{1,2}$ depend crucially on the dependent variables $\{x_i, \dot{x}_i\}$ at the start of each interval $[t_i, t_{i+1})$. If the time axis is so partially ordered as to consist of a countable infinity of real intervals $[t_i, t_{i+1})$, $i = 0, 1, 2, \ldots$, then it is possible to obtain a countable infinity of periodic and non-periodic orbits (all saddle type) via the present linearization procedure as the time marching is continued. At this stage, it may be recalled that a chaotic orbit may be visualized as being made up of a countable infinity of unstable periodic orbits and an uncountable infinity of unstable non-periodic orbits. Such an observation hints at the possibility of simulating a chaotic trajectory to high precision through the PSL technique. However, since the time axis can only be ordered into a countable number of subdivisions, a countable set of non-periodic orbits can be generated in practice.

Now it would be interesting to verify the performance of the linearization scheme against numerical simulations of subharmonic, quasi-periodic and chaotic response of Ueda's, Duffing-Holmes' and Van der Pol's oscillators. While Ueda's oscillator shows a period doubled subharmonic route to chaos, for the Duffing-Holmes oscillator chaos ensues due to homoclinic bifurcation followed by destruction of the separatrix structure in the phase plane. In contrast, a complicated motion, such as quasi-periodicity or chaos, may ensue in Van der Pol's oscillator due to interaction between the self-excited limit cycle and the external periodic forcing. All the numerical solutions have been obtained using both the PSL and fourth order Runge-Kutta schemes. The time step for integration has been uniformly fixed at $\Delta t = 0{\cdot}005$ unless specifically mentioned to the contrary. First, various subharmonic orbits of Ueda's oscillator are shown in Figure 1. In Figure 2, a chaotic orbit of Ueda's oscillator as computed using PSL and Runge-Kutta schemes is reported. For the Duffing-Holmes oscillator, again, the results of a set of simulations of subharmonic orbits are shown in Figure 3. Simulated chaotic orbits for this oscillator are shown in Figure 4. Finally, for the Van der Pol oscillator, a quasi-periodic orbit is shown in Figure 5. The orbit is seen to be filling up the phase plane due to irrational frequency ratio(s) in the response process. However, present attempts to find chaotic regimes for this oscillator have not proved fruitful. On the other hand, if a combined Van der Pol's and Duffing-Holmes' type of oscillator with the following form

$$\ddot{x} + 2\pi\varepsilon_1(4x^2 - 1)\dot{x} + 4\pi^2\varepsilon_2(x^3 - x) = 4\pi^2\varepsilon_3 \cos(2\pi t) \tag{5}$$

is chosen, then chaos is a distinct possibility due to a complicated interaction between the limit cycle and the homoclinic orbit. One such orbit, computed by using both linearization and Runge-Kutta schemes, is reported in Figure 6. From the shape of the chaotic orbit as projected onto the phase plane it may be inferred that for this oscillator chaos occurs in the form of a noisy limit cycle with intermittent chaotic bursts, i.e., on the line of the Pomeau-Manneville scenario.

3. DUFFING-HOLMES OSCILLATOR: FORCED SEPARATRIX

The forced separatrix corresponds to the forced stable manifold. That such a forced stable manifold exists for sufficiently small values of the perturbation parameters, ε_1 and ε_3, follows from the invariant manifold theory [9]. As in the derivation of the unstable limit cycle, described in the companion paper [1], here again it would be convenient to consider the oscillator after introducing a phase, ϕ, in the forcing term. Thus, the equation is

$$\ddot{x} + 2\pi\varepsilon_1\dot{x} + 4\pi^2\varepsilon_2(x^3 - x) = 4\pi^2\varepsilon_3 \cos 2\pi(t + \phi). \tag{6}$$

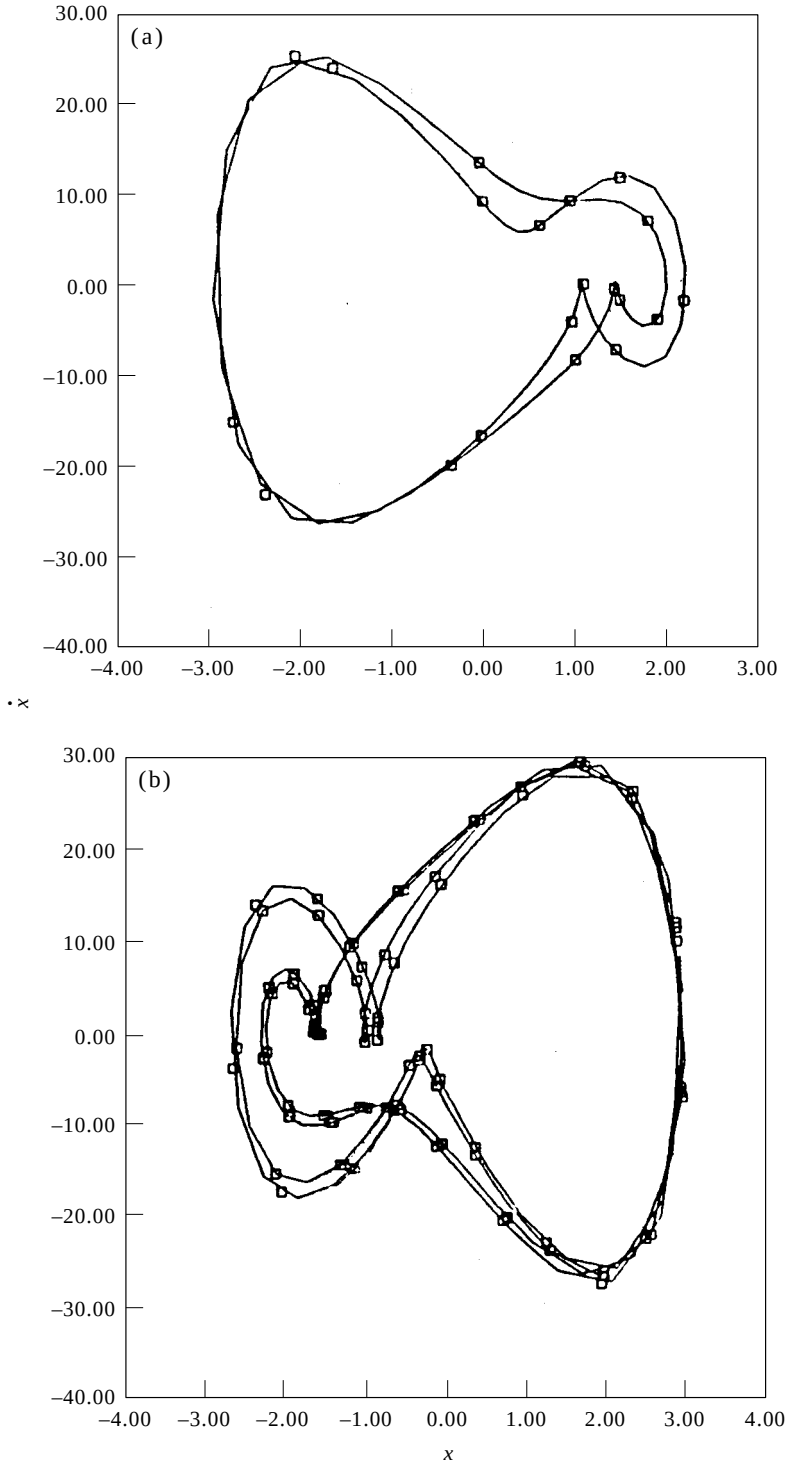

Figure 1. Subharmonic orbits of Ueda's oscillator: (a) two-periodic orbit, $\epsilon_1 = 0{\cdot}25$, $\epsilon_2 = 1{\cdot}0$, $\epsilon_3 = 2{\cdot}0$; (b) four-periodic orbit, $\epsilon_1 = 0{\cdot}25$, $\epsilon_2 = 1{\cdot}0$, $\epsilon_3 = 7{\cdot}0$, □□□□, Runge-Kutta; ——, linearization.

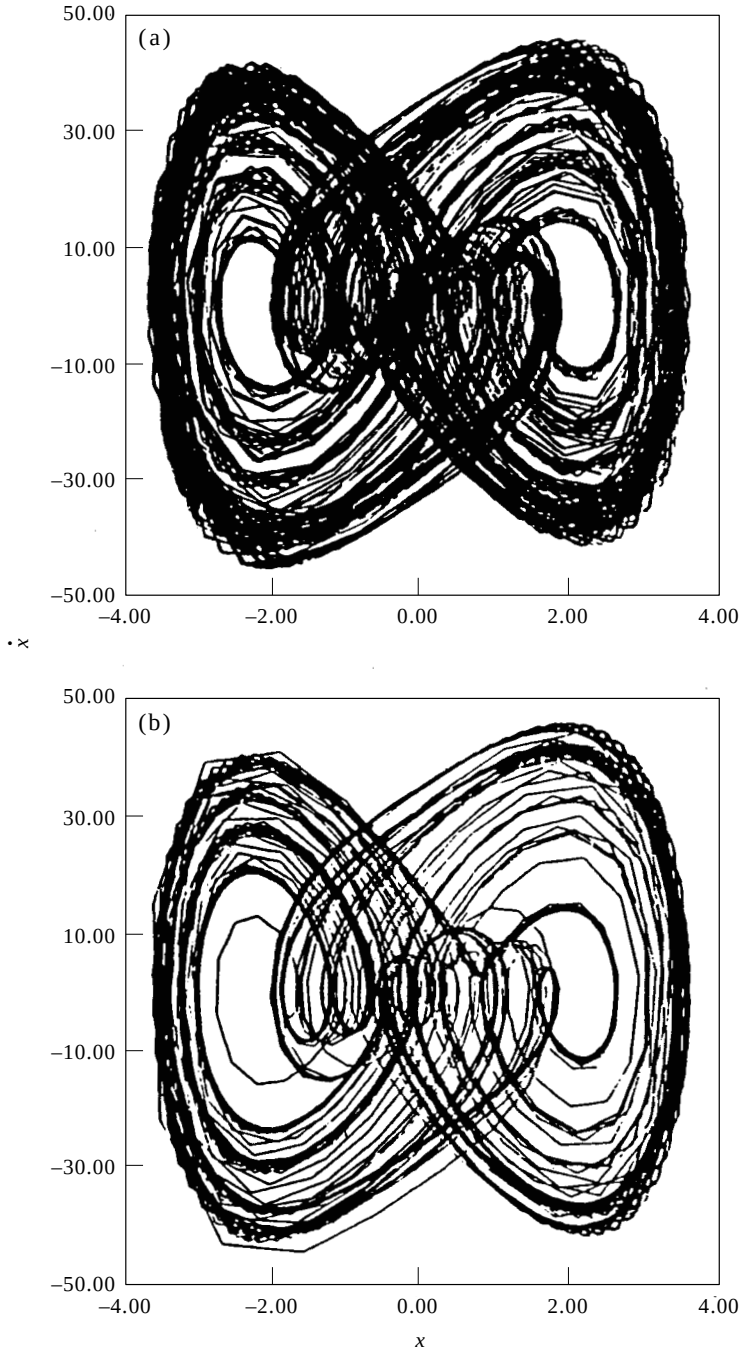

Figure 2. A chaotic orbit of Ueda's oscillator, $\varepsilon_1 = 0{\cdot}25$, $\varepsilon_2 = 1{\cdot}0$, $\varepsilon_3 = 11{\cdot}0$: (a) linearization; (b) Runge-Kutta.

At the outset, it is required to find out a point $\{{}^u x_i, {}^u \dot{x}_i, {}^u \phi_i\}$ on the unstable limit cycle as explained in the previous paper. Since the eigenvalues ${}^i\lambda_{1,2}$ are real near this point, the solution for the forced separatrix passing through $\{{}^u x_i, {}^u \dot{x}_i\}$ may be written down as

$$x_{j+1} = x_j + \Delta_j = K_{2j} \exp\{{}^j\lambda_2(x_j, \Delta_j)h_j\} + p(t_{j+1}, \phi_j), \tag{7}$$

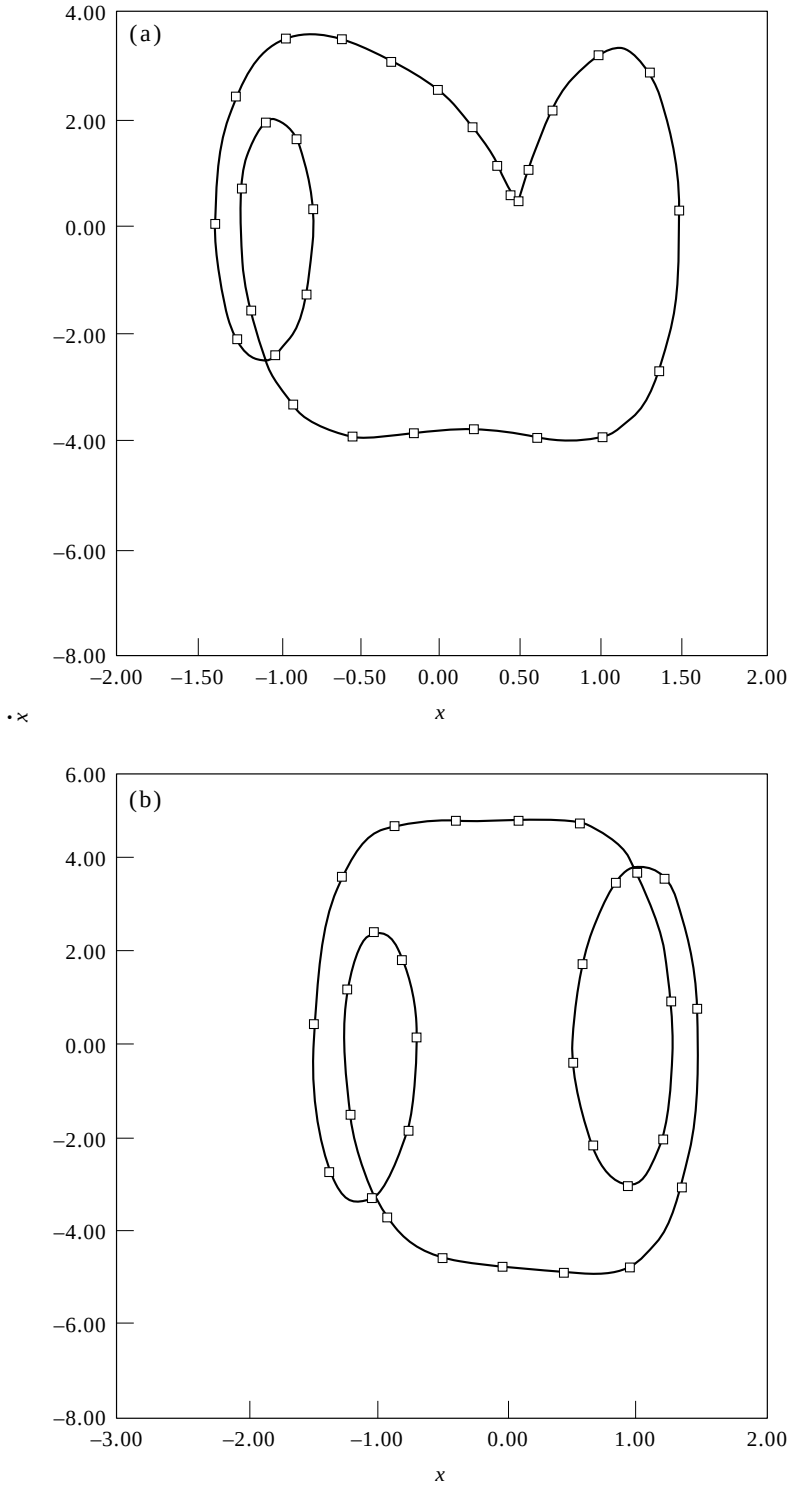

Figure 3. Subharmonic orbits of Duffing-Holmes' oscillator: (a) two-periodic orbit, $\varepsilon_1 = 0{\cdot}25$, $\varepsilon_2 = 0{\cdot}5$, $\varepsilon_3 = 0{\cdot}3$; ——, Runge-Kutta; □□□□, linearization. (b) Three-periodic orbit, $\varepsilon_1 = 0{\cdot}25$, $\varepsilon_2 = 0{\cdot}5$, $\varepsilon_3 = 0{\cdot}4$; ——, Linearization: □□□□, Runge-Kutta.

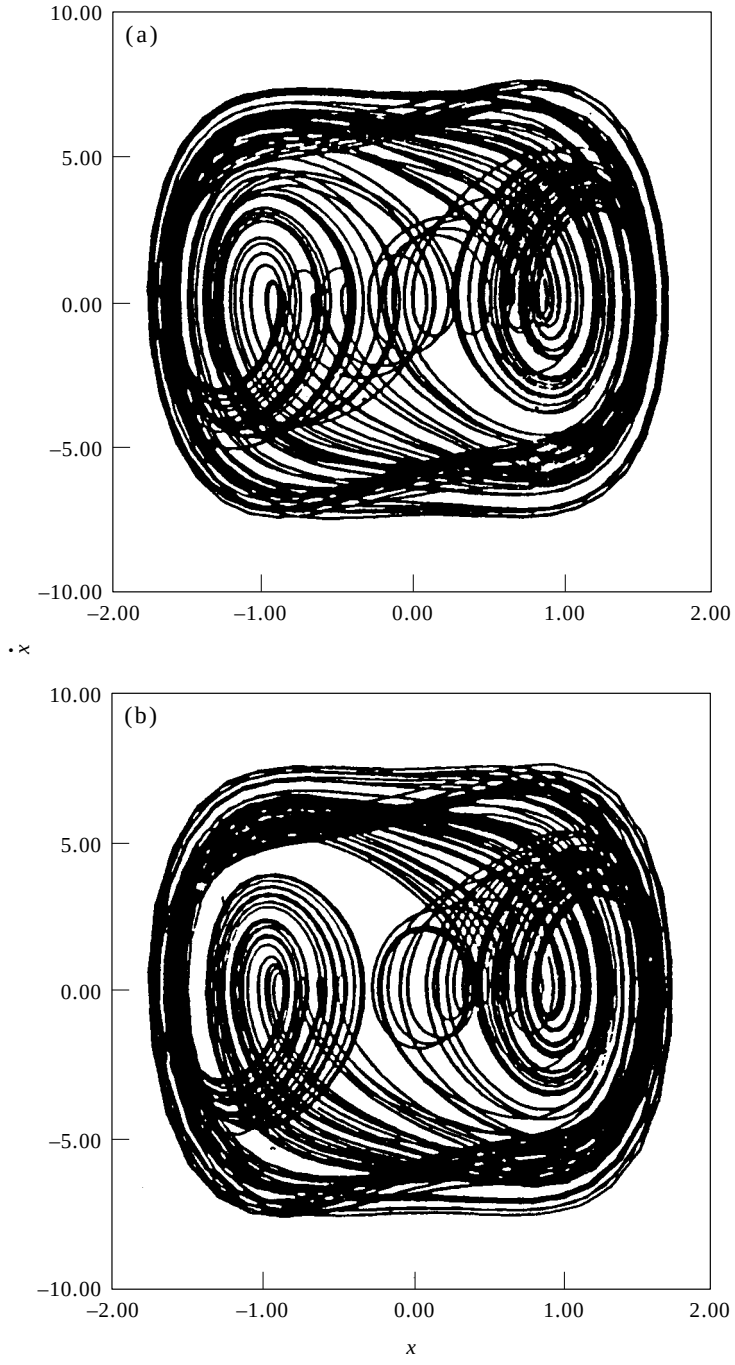
(a)
10.00
5.00
0.00
−5.00
−10.00
−2.00
−1.00
0.00
1.00
2.00
ẋ
(b)
10.00
5.00
0.00
−5.00
−10.00
−2.00
−1.00
0.00
1.00
2.00
x

Figure 4(a)–(b)

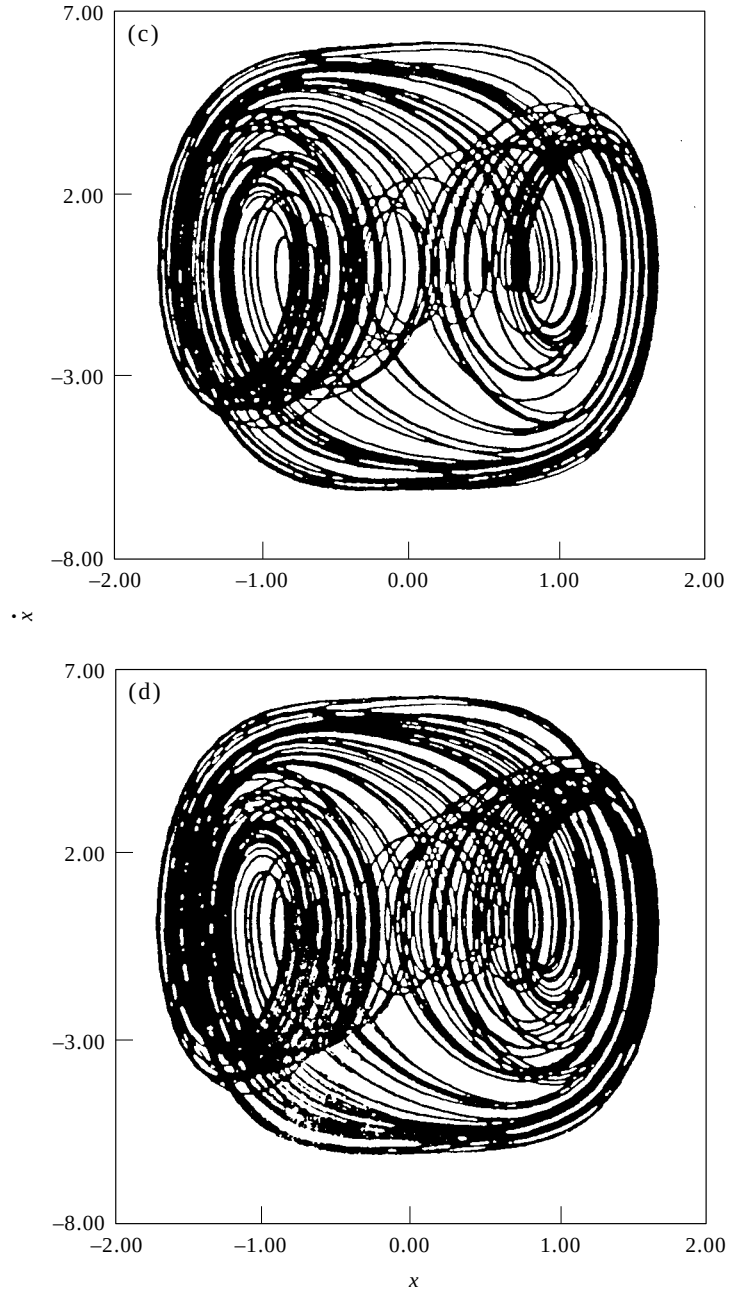

Figure 4(c)–(d)

Figure 4. Chaotic orbits of Duffing-Holmes' oscillator: (a) via linearization, $\varepsilon_1 = 0{\cdot}25$, $\varepsilon_2 = 0{\cdot}5$, $\varepsilon_3 = 0{\cdot}5$; (b) via Runge-Kutta, $\varepsilon_1 = 0{\cdot}25$, $\varepsilon_2 = 0{\cdot}5$, $\varepsilon_3 = 0{\cdot}5$; (c) via linearization, $\varepsilon_1 = 0{\cdot}25$, $\varepsilon_2 = 0{\cdot}3$, $\varepsilon_3 = 0{\cdot}45$; (d) via Runge-Kutta, $\varepsilon_1 = 0{\cdot}25$, $\varepsilon_2 = 0{\cdot}3$, $\varepsilon_3 = 0{\cdot}45$.

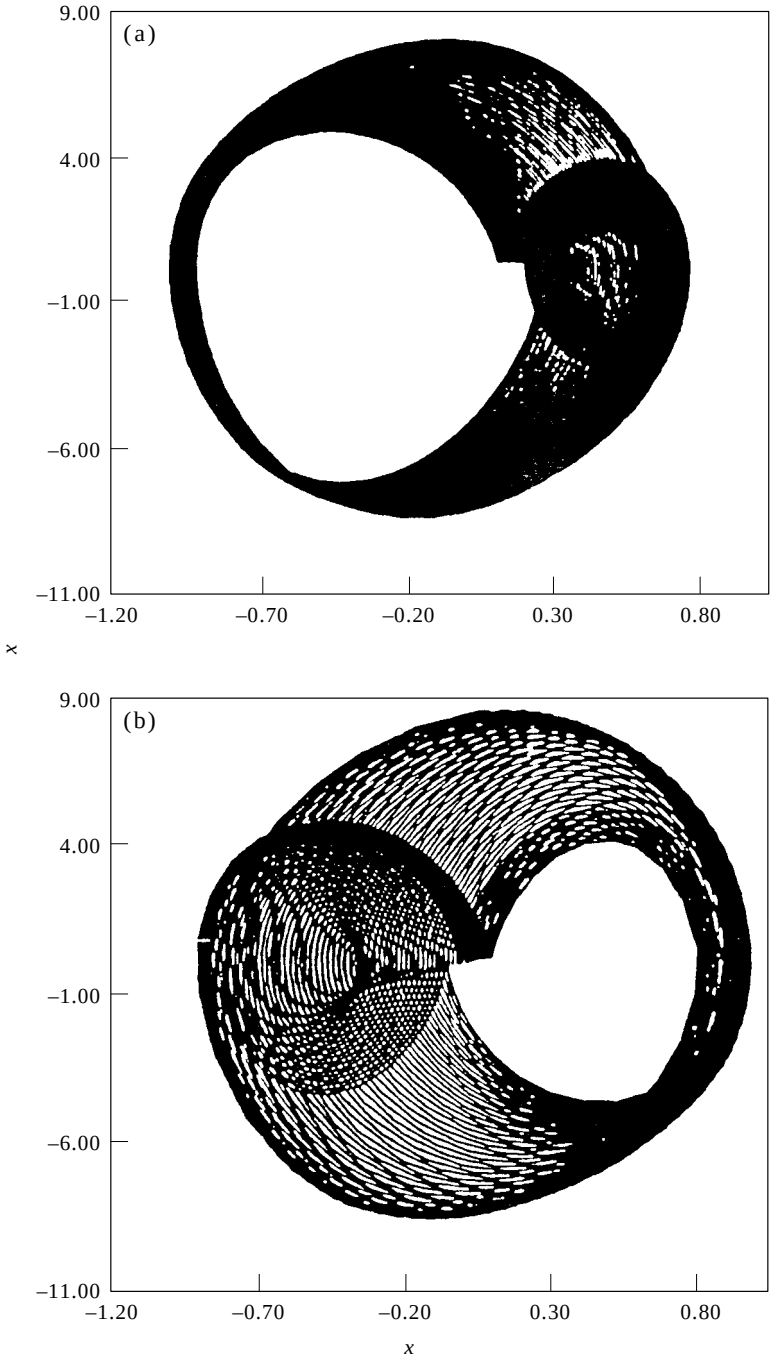

Figure 5. A quasi-periodic orbit of Van der Pol's oscillator, $\varepsilon_1 = 0{\cdot}25$, $\varepsilon_2 = 4{\cdot}0$, $\varepsilon_3 = 2{\cdot}0$: (a) via linearization; (b) via Runge-Kutta.

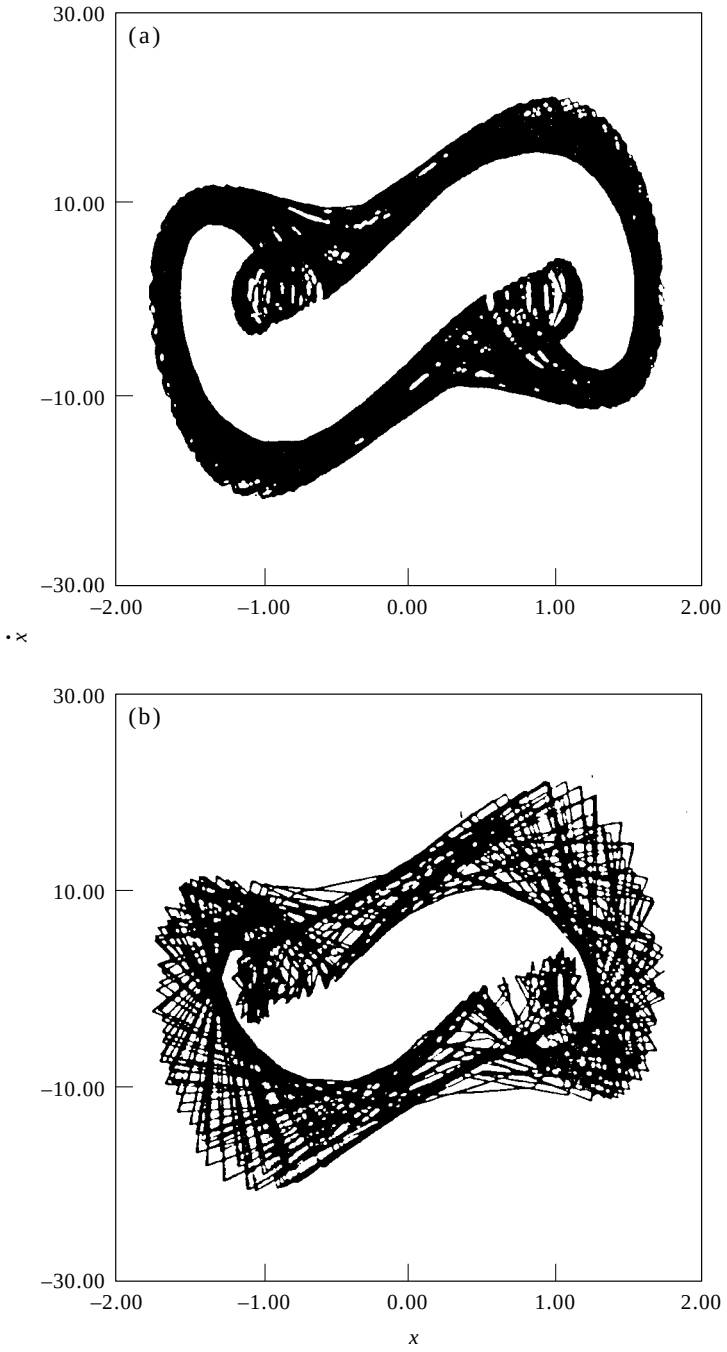

Figure 6. A chaotic orbit of combined Duffing-Holmes' and Van der Pol's oscillator, $\varepsilon_1 = 0{\cdot}25$, $\varepsilon_2 = 4{\cdot}0$, $\varepsilon_3 = 3{\cdot}0$: (a) via linearization; (b) via Rung-Kutta.

where

$$x_j = {}^u x_i,$$

$$\dot{x}_j = {}^u \dot{x}_i,$$

$$p(t_{j+1}, \phi_j) = (1/D)\varepsilon_3[\varepsilon_2\{\beta(x_j, \Delta_j) - 1\} - 1] \cos 2\pi(t_{j+1} + \phi_i)$$

$$+ (1/D)\varepsilon_1\varepsilon_3 \sin 2\pi(t_{j+1} + \phi_i),$$

$$K_{20} = {}^u x_i - p(0, {}^u\phi_i),$$

$$\beta(x_j, \Delta_j) = \frac{(x_j^4 + 2x_j^3\Delta_j + 2x_j^2\Delta_j^2 + x_j\Delta_j^3 + \Delta_j^4/5)}{(x_j^2 + x_j\Delta_j + \Delta_j^2/3)},$$

$$D = \{\varepsilon_2(\beta - 1) - 1\}^2 + \varepsilon_1^2,$$

$$h_j = t_{j+1} - t_j. \tag{8}$$

Thus the value of K_{20} is seen to be dependent on the choice of the point on the unstable limit cycle, from which the separatrix emerges backwards in time. Since the limit cycle itself consists of an uncountable infinity of points, an uncountable infinity of forced separatrices can (theoretically) be constructed using the PSL method. Equation (7) may be used to move backwards in time till ${}^j\lambda_2$ becomes complex. In this case, the last obtained values of x_j and $\dot{x}_j$ should be used to move further backwards in time. It may be mentioned here that the methodology for obtaining the unstable manifold of the perturbed homoclinic orbit also follows the same pattern as for the perturbed stable manifold. The only difference in this case is that the complementary function in equation (7) should be constructed with the positive eigenvalue, ${}^j\lambda_1$, instead of the negative eigenvalue, ${}^j\lambda_2$.

As a numerical illustration for the above procedure, the stable and unstable manifolds, denoted respectively by ${}^cW_s$ and ${}^cW_u$, are plotted in Figure 7 for different values of ϵ_3. It is clearly demonstrated that for some specific value of ϵ_3 at a Poincaré section based at $\phi = \phi_i$, a quadratic tangency between the stable and unstable manifolds occurs, as predicted by the Melnikov function. The forced separatrix, which constitutes the stable manifold normally hyperbolic to the unstable limit cycle and separates the basins of attraction of the two stable limit cycles, is plotted in Figure 8. Here the procedure for constructing the forced separatrix follows a similar pattern as for constructing the stable manifold. First, a set of points $(\{{}^u x_i, {}^u\dot{x}_i, \phi_i | i = 1, 2, \ldots)$ on the unstable limit cycle is found. Then any point $\{{}^u x_j, {}^u\dot{x}_j, \phi_j\}$ on this orbit is chosen. This point serves as the limit point of the corresponding separatrix as $t \to \infty$ based on a Poincaré section Σ_{ϕ_i} at ϕ_i. Next, both the branches of the stable manifold originating from this point may be constructed by considering the local eigenvalue structure of the equivalent linear flow as obtained via the PSL.

4. ONSET OF CHAOTIC DIFFUSION

A necessary condition for the onset of chaos in the Duffing-Holmes oscillator may be obtained using the Melnikov criterion. However, this is not a sufficient condition since the Melnikov boundary only predicts the minimum possible parameter combinations below which chaos is not possible. On the other hand, it is possible to use the analytical expressions for the stable and unstable one-periodic orbits via PSL to heuristically argue out a sufficient condition for the onset of steady-state chaos. It is known that these orbits

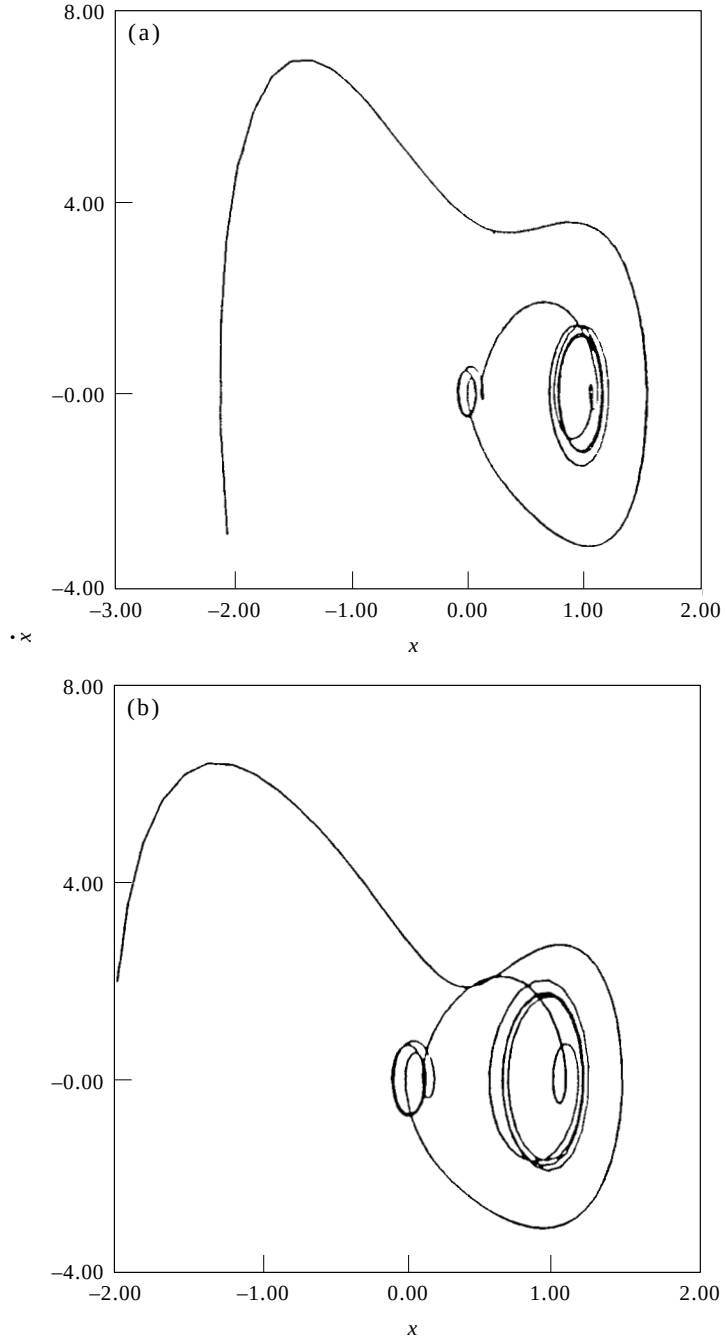

Figure 7. Stable and unstable manifolds of the unstable periodic orbit of the forced Duffing-Holmes oscillator: (a) $\varepsilon_1 = 0{\cdot}25$, $\varepsilon_2 = 0{\cdot}5$, $\varepsilon_3 = 0{\cdot}1$; (b) $\varepsilon_1 = 0{\cdot}25$, $\varepsilon_2 = 0{\cdot}5$, $\varepsilon_3 = 0{\cdot}25$.

are invariant solution manifolds. The stable and unstable one-periodic orbits cannot, therefore, intersect each other, since such an intersection would violate the uniqueness condition of the solution trajectories. It may also be argued that given a set of values for

the damping and stiffness parameters, namely ε_1 and ε_2, it is possible for all the three one-periodic orbits to co-exist for sufficiently low values of the forcing amplitude parameter, ε_3. Now, as ε_3 is slowly increased, the size of each of these orbits also increases. Thus, with increase in ε_3, the unstable and stable orbits come closer and closer. Let d be the minimum distance of separation of any two points, one on the unstable limit cycle and the other on any one of the stable limit cycles. Consider, for example, the stable limit cycle with positive x, if $\{{}^{s}x_{min}, 0\}$ is the co-ordinate of the point of intersection of this orbit with the x-axis towards the origin, then d would be given by

$$d = {}^{s}x_{min} - {}^{u}x_{max}, \qquad \text{with} \qquad 0 < {}^{u}x_{max} < {}^{s}x_{min} < 1. \tag{9}$$

A sufficient condition for a quadratic tangency of the stable and unstable limit cycles is that $d = 0$. However, this is not a necessary condition since phase information is lost in the phase plane representation. Let the parameter ε_3 be denoted as ${}^{c}\varepsilon_3$ when $d = 0$. It is evident that at this stage, the double-well potential structure of the Duffing-Holmes oscillator may break down due to the non-existence of the unstable limit cycle and thus a chaotic diffusion may set in. The idea as presented above is not new and has already been hinted at by Dowell and Pezeshki [10]. However, further efforts at obtaining the corresponding boundary accurately in the parameter space have been frustrated by the lack of proper methodologies to produce the stable and unstable limit cycles analytically. It may also be mentioned that even before a quadratic tangency of the stable and unstable limit cycles can occur, chaos is likely to set in following a particular type of instability of the small one-periodic orbits [11]. However, it is of interest to investigate the ranges of

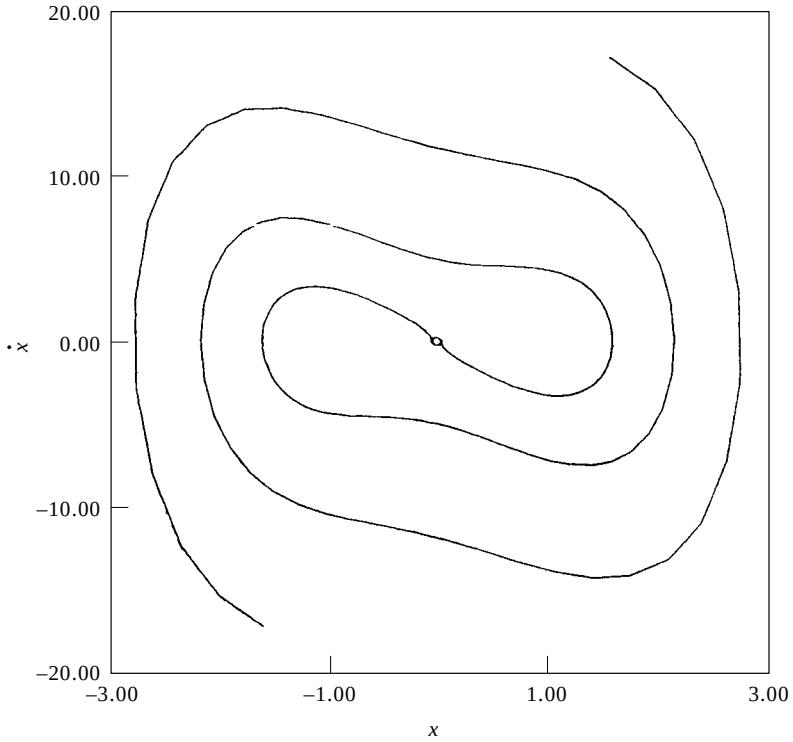

Figure 8. Forced separatrix of Duffing-Holmes' oscillator, $\varepsilon_1 = 0{\cdot}25$, $\varepsilon_2 = 0{\cdot}5$, $\varepsilon_3 = 0{\cdot}05$.

parameters for which $d \to 0$, as this gives an upper bound in the parameter plane below which a quadratic tangency of the stable and unstable limit cycles is not possible.

An analytical treatment of the unstable limit cycle via PSL was performed in the companion paper [1]. Now a similar treatment is possible for the stable limit cycles. To this end, the following transformation would be useful

$$x = y + 1. \tag{10}$$

In this new variable y, the Duffing-Holmes equation becomes

$$\ddot{y} + 2\pi\varepsilon_1\dot{y} + 4\pi^2\varepsilon_2(y^2 + 3y + 2)y = 4\pi^2\varepsilon_3 \cos 2\pi(t + \phi). \tag{11}$$

When $\varepsilon_3 = 0$, $\{0, 0\}$ and $\{-2, 0\}$ are stable sinks and $\{-1, 0\}$ is an unstable saddle for the above equation. Here the orbits of the stable limit cycles would be around $\{0, 0\}$ and $\{-2, 0\}$ in the phase plane. Now, the equivalent linear form for this equation may be written down as

$$\ddot{y} + 2\pi\varepsilon_1\dot{y} + 4\pi^2\varepsilon_2\kappa(y_i, \Delta_i)y = 4\pi^2\varepsilon_3 \cos 2\pi(t + \phi). \tag{12}$$

The coefficient κ may be found by an error minimization over the segment $[y_i, y_{i+1})$. Moreover, it may be readily verified that

$$\lim_{\Delta_i \to 0} \kappa(y_i, \Delta_i) = y_i^2 + 3y_i + 2. \tag{13}$$

It may also be mentioned that the function $\kappa(y_i, 0)$ is positive for all $y_i > -1$. Thus, if attention is focused on finding the stable limit cycle lying on the right hand side of the unstable limit cycle, then the real parts of the eigenvalues of the complementary part of equation (11) on and around the stable limit cycle would always be negative. Hence, following the same arguments as presented in the companion paper [1], a transcendental equation for the x-co-ordinate of any point $\{{}^s y_i, {}^s \dot{y}_i\}$ lying on the right-hand-side stable limit cycle may be found to be

$${}^s y_i = \frac{1}{D}\left[\varepsilon_3\{\varepsilon_2({}^s y_i^2 + 3{}^s y_i + 2) - 1\} \cos(2\pi\phi_i) + \varepsilon_1\varepsilon_3 \sin(2\pi\phi_i)\right]. \tag{14}$$

The above equation needs to be solved for various $\phi_i \in [0, 1)$ to obtain the complete limit cycle. The co-ordinate ${}^s \dot{y}_i$ may be found out by simply differentiating the above equation with respect to ϕ. This gives

$${}^s \dot{y}_i = -\frac{2\pi}{D}\left[\varepsilon_3\{\varepsilon_2({}^s y_i^2 + 3{}^s y_i + 2) - 1\} \sin(2\pi\phi_i) - \varepsilon_1\varepsilon_3 \cos(2\pi\phi_i)\right]. \tag{15}$$

The stable one-periodic orbits of the Duffing-Holmes oscillator have been constructed analytically following the procedure outlined above for various parameter combinations. These orbits, along with the numerically simulated ones, are shown in Figure 9. It is seen that the comparison is favourable. Next, to study the structure of near-tangency of the stable and unstable limit cycles, the curve of ${}^c\varepsilon_3$ versus ε_2 is plotted in Figure 10. In this figure, the hatched region, which has been delineated by computing the highest Liapunov exponent followed by a positivity check, is chaotic [12]. It is thus seen that even below the boundary for near-tangency of the stable and unstable one-periodic orbits, chaos is possible in the Duffing-Holmes oscillator.

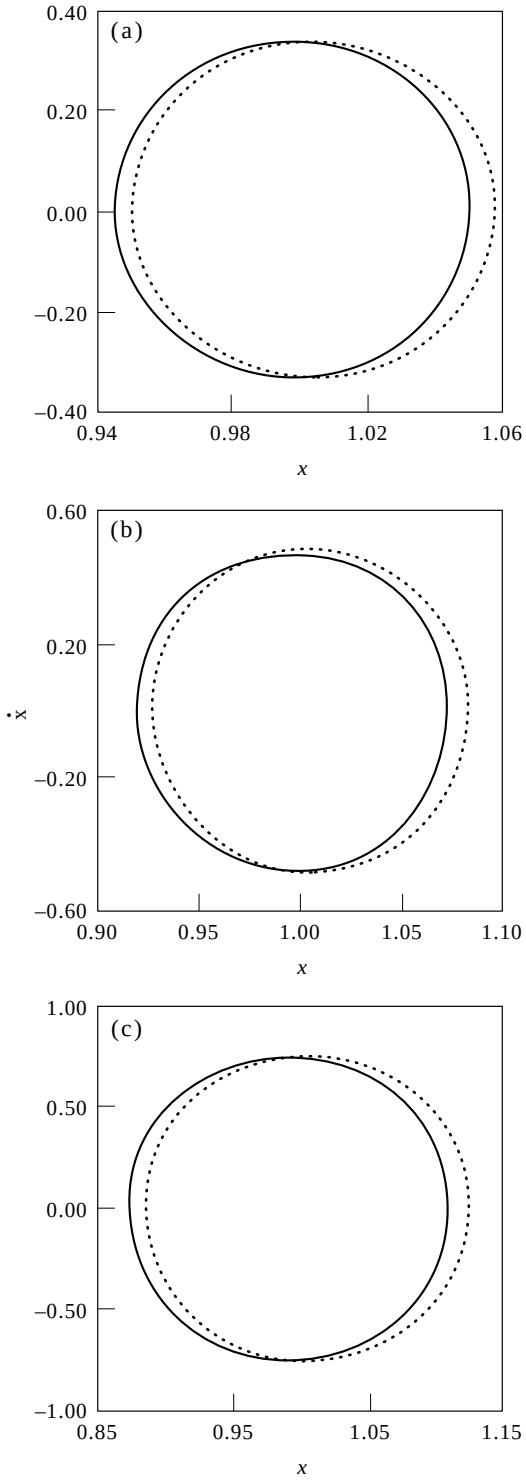

Figure 9. Small one-periodic orbits of forced Duffing-Holmes' oscillator: (a) $\varepsilon_1 = 0{\cdot}25$, $\varepsilon_2 = 0{\cdot}3$, $\varepsilon_3 = 0{\cdot}025$; (b) $\varepsilon_1 = 0{\cdot}25$, $\varepsilon_2 = 0{\cdot}2$, $\varepsilon_3 = 0{\cdot}05$; (c) $\varepsilon_1 = 0{\cdot}25$, $\varepsilon_2 = 0{\cdot}1$, $\varepsilon_3 = 0{\cdot}1$. · · · · , Analytical; ——, simulation.

5. FOURIER SPECTRA

The fact that the local flow structure for non-linear oscillators is explicitly known in terms of a continuous function in the PSL method may be exploited to compute the Fourier spectra. Let $X(t)$ denote a trajectory of a non-linear ODE of the form of equation (1). To obtain the Fourier spectrum of $X(t)$, the following Fourier inversion

$$S(\omega) = S_1(\omega) + S_2(\omega), \tag{16}$$

where

$$S_1(\omega) = \lim_{T\to\infty} \int_0^T X(t) \cos(\omega t)\, \mathrm{d}t,$$

$$S_2(\omega) = \lim_{T\to\infty} \int_0^T X(t) \sin(\omega t)\, \mathrm{d}t, \tag{17}$$

is performed. Once the above quantities are known, it suffices to obtain the Fourier amplitude,

$$A(\omega) = \sqrt{S_1^2(\omega) + S_2^2(\omega)}. \tag{18}$$

Now, according to the present method of linearization, the complete solution trajectory, $X(t)$, is given by

$$X(t) = \bigcup_{\forall i} \{{}^i x(t) \mid t \in [t_i, t_{i+1})\}, \tag{19}$$

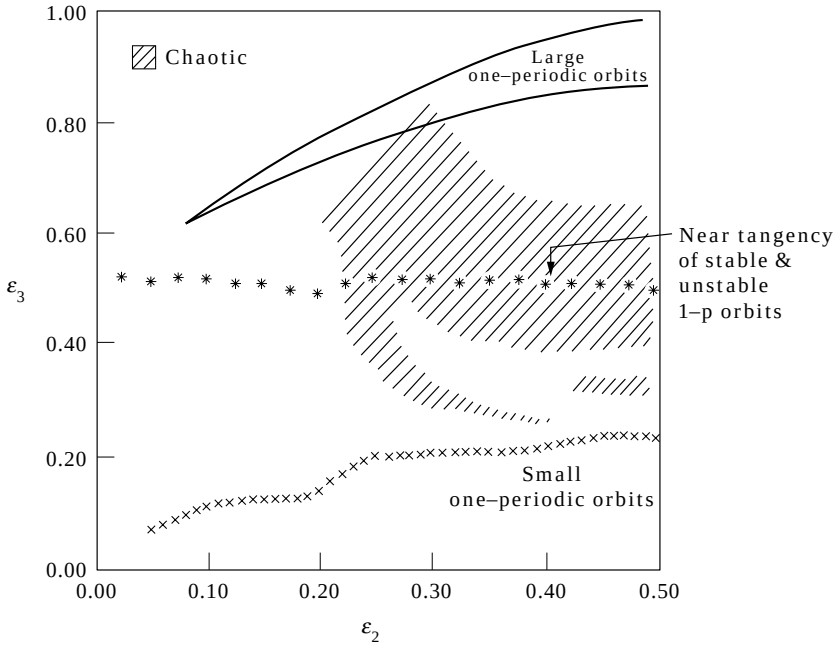

Figure 10. A partially structured ε_3–ε_2 plane, $\varepsilon_1 = 0{\cdot}25$.

where ${}^{i}x(t)$ is the solution of the linear ODE valid over $[t_i, t_{i+1})$. Thus, the integrations required to be performed in equation (17) can be equivalently written as

$$S_1(\omega) = \lim_{N\to\infty} \sum_{i=0}^{N} \frac{1}{h_i} \int_{t_i}^{t_{i+1}} x(t) \cos(\omega t)\, \mathrm{d}t,$$

$$S_2(\omega) = \lim_{N\to\infty} \sum_{i=0}^{N} \frac{1}{h_i} \int_{t_i}^{t_{i+1}} x(t) \sin(\omega t)\, \mathrm{d}t. \tag{20}$$

since the solution for ${}^{i}x(t)$ is known in closed form and is in terms of only exponential and trigonometric functions, the above integrals can also be obtained in closed form. Thus, taking for instance the Duffing-Holmes oscillator, if ${}^{i}\lambda_{1,2}$ are real, then

$$\begin{aligned}
\int_{t_i}^{t_{i+1}} {}^{i}x(t) \cos(\omega t)\, \mathrm{d}t = {} & \{K_{1i}/({}^{i}\lambda_1^2 + \omega^2)\}[\exp({}^{i}\lambda_1 h_i)\{{}^{i}\lambda_1 \cos(\omega t_{i+1}) \\
& + \omega \sin(\omega t_{i+1})\} - \{{}^{i}\lambda_1 \cos(\omega t_i) + \omega \sin(\omega t_i)\}] \\
& \{K_{2i}/({}^{i}\lambda_2^2 + \omega^2)\}[\exp({}^{i}\lambda_2 h_i\{{}^{i}\lambda_2 \cos(\omega t_{i+1}) + \omega \sin(\omega t_{i+1})\} \\
& - \{{}^{i}\lambda_2 \cos(\omega t_i) + \omega \sin(\omega t_i)\}] \\
& + \{G_1/2(2\pi + \omega)\}[\sin(2\pi + \omega)t_{i+1} \\
& - \sin(2\pi + \omega)t_i] + \{G_1/2(2\pi - \omega)\}[\sin(2\pi - \omega)t_{i+1} \\
& - \sin(2\pi - \omega)t_i] \\
& - \{G_2/2(2\pi + \omega)\}[\cos(2\pi + \omega)t_{i+1} - \cos(2\pi + \omega)t_i] \\
& - \{G_2/2(2\pi - \omega)\}[\cos(2\pi - \omega)t_{i+1} - \cos(2\pi - \omega)t_i],
\end{aligned} \tag{21}$$

and,

$$\begin{aligned}
\int_{t_i}^{t_{i+1}} {}^{i}x(t) \sin(\omega t)\, \mathrm{d}t = {} & \{K_{1i}/({}^{i}\lambda_1^2 + \omega^2)\}[\exp({}^{i}\lambda_1 h_i)\{{}^{i}\lambda_1 \sin(\omega t_{i+1}) \\
& - \omega \cos(\omega t_{i+1})\} - \{{}^{i}\lambda_1 \sin(\omega t_i) + \omega \cos(\omega t_i)\}] \\
& - \{G_1/2(2\pi + \omega)\}[\cos(2\pi + \omega)t_{i+1} - \cos(2\pi + \omega)t_i] \\
& + \{G_1/2(\omega - 2\pi)\}[\cos(\omega - 2\pi)t_{i+1} - \cos(\omega - 2\pi)t_i] \\
& + \{G_2/2(\omega - 2\pi)\}[\sin(\omega - 2\pi)t_{i+1} - \sin(\omega - 2\pi)t_i] \\
& - \{G_2/2(2\pi + \omega)\}[\sin(2\pi + \omega)t_{i+1} - \sin(2\pi + \omega)t_i],
\end{aligned} \tag{22}$$

where

$$G_1 = \frac{\varepsilon_3\{\varepsilon_2\beta(x_i) - 1\}}{[\{\varepsilon_2\beta(x_i) - 1\}^2 + \varepsilon_1^2]} \tag{23}$$

and,

$$G_2 = \frac{\varepsilon_1\varepsilon_3}{[\{\varepsilon_2\beta(x_i) - 1\}^2 + \varepsilon_1^2]}. \tag{24}$$

Similar calculations can be performed for the case where ${}^i\lambda_{1,2}$ are complex conjugates. An advantage of the presently adopted technique of Fourier inversion is that the trajectory $X(t)$ in between any pair of points $\{x_i, \dot{x}_i\}$ and $\{x_{i+1}, \dot{x}_{i+1}\}$ is locally simulated by a C^∞ curve. This is in sharp contrast with the usual procedure of generating a finite number of data points by numerical integration schemes and then evaluating the integrals in (17) by using approximate schemes such as the Gaussian quadrature or the five point rule.

In Figure 11, the Fourier spectra of the Duffing-Holmes oscillator for a periodic and a chaotic case is shown using the PSL scheme as outlined above. As expected, for the one-periodic case, there is only one sharp peak at the frequency of the external forcing. However, for the chaotic case, a broad-banded spectrum is realized. A noticeable feature of chaos here is the persistence of a sharp peak at the frequency of the external forcing. This means that the chaotic trajectory spends a considerable time near the one-periodic orbit.

6. LIAPUNOV CHARACTERISTIC EXPONENTS (LCEs)

Two different methods are presented here to compute the LCEs of a non-linear oscillator using the PSL approach. While the first method extracts the exponents by treating the local solution over a small segment of the trajectory as a map, the second method makes use of the local eigenvalue structure of an error-minimized variational equation to extract all the exponents.

6.1. METHOD 1

In the companion paper [1], it was shown that it is possible to reduce the flow of a second order non-linear ODE to a 2-D non-linear map using the concept of piecewise linearization. Thus, considering the oscillator in equation (1), the following non-linear map may be arrived at:

$$x_{i+1} = F_{1i}(x_i, \dot{x}_i, \Delta_i, t_{i+1}, h_i),$$
$$\dot{x}_{i+1} = F_{2i}(x_i, \dot{x}_i, \Delta_i, t_{i+1}, h_i). \tag{25}$$

The detailed derivation for the functions F_{1i} and F_{2i} was performed in the companion paper [1] and hence is not reproduced here. Now, the explicit form of the above non-linear map may be readily exploited to generate all the LCEs of the original ODE (1). If the time-step, h_i, is kept constant at $h_i = h$, then the map (25) may be construed as 2-D Poincaré section over an interval h of the ODE (1), which in turn is equivalent to a 3-D autonomous ODE. Thus, in principle, the two LCEs of the map should be the same as the two non-zero LCEs of the original non-linear equation. Now, adopting the usual approach for computing the LCEs of a map, let $\Gamma_i(n)$, $i = 1, 2, \ldots$, be the eigenvalues of the matrix

$$B_n = [M_n \cdot M_{n-1} \cdots M_1]^{1/n}, \tag{26}$$

where

$$M_j = \begin{bmatrix} \dfrac{\partial F_{1j}}{\partial^j x_j} & \dfrac{\partial F_{1j}}{\partial^j \dot{x}_j} \\ \dfrac{\partial F_{2j}}{\partial^j x_j} & \dfrac{\partial F_{2j}}{\partial^j \dot{x}_j} \end{bmatrix}. \tag{27}$$

Then the non-zero LCEs of the non-linear ODE are given by

$$\sigma_i = \lim_{n \to \infty} \ln |\Gamma_i(n)|. \tag{28}$$

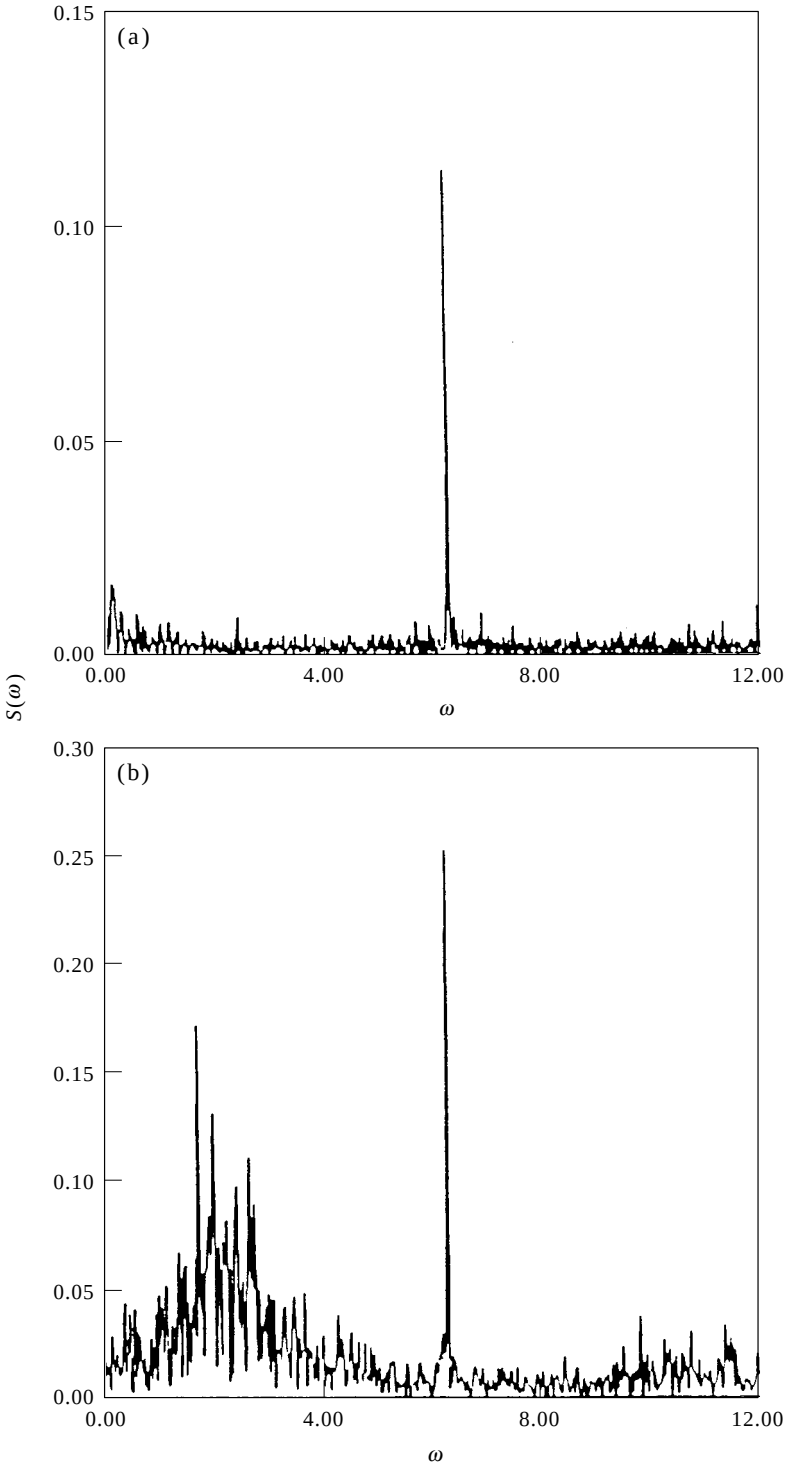

Figure 11. Fourier spectra for Duffing-Holmes' oscillator: (a) one-periodic case, $\varepsilon_1 = 0{\cdot}25$, $\varepsilon_2 = 0{\cdot}5$, $\varepsilon_3 = 0{\cdot}1$; (b) chaotic case, $\varepsilon_1 = 0{\cdot}25$, $\varepsilon_2 = 0{\cdot}3$, $\varepsilon_3 = 0{\cdot}45$.

The third LCE of the non-linear ODE (1) is identically zero. However, it may be noted that due to the complicated nature of the functions F_{1j} and F_{2j}, it may sometimes be laborious to manually compute the partial derivatives to construct the matrix M_j. For such cases, it would be convenient to compute the derivatives symbolically using computer programmes such as MATLAB.

To compare the LCEs obtained using the above scheme with those obtained using existing standard techniques, an algorithm introduced by Iyengar [12] to compute the maximum LCE is made use of. The first variational equation of the Duffing-Holmes oscillator is given by

$$\ddot{v} + 2\pi\varepsilon_1\dot{v} - 4\pi^2\varepsilon_2(1 - 3x^2)v = 0. \tag{29}$$

Now, introducing the polar transformation

$$v = \exp(-\pi\varepsilon_1 t)r\cos\phi,$$

$$\dot{v} = \exp(-\pi\varepsilon_1 t)r(\sin\phi - \pi\varepsilon_1\cos\phi), \tag{30}$$

one gets

$$\dot{r} = 0{\cdot}5(1 + 4\pi^2\varepsilon_2 + \pi^2\varepsilon_1^2 - 12\pi^2\varepsilon_2 x^2)r\sin(2\phi),$$

$$\dot{\phi} = -1 + 0{\cdot}5(1 + 4\pi^2\varepsilon_2 + \pi^2\varepsilon_1^2 - 12\pi^2\varepsilon_2 x^2)\{1 + \cos(2\phi)\}. \tag{31}$$

The maximum LCE is now given by

$$\sigma_{max} = \lim_{T\to\infty}\left[-\pi\varepsilon_1 + \frac{1}{2T}\int_0^T (1 + \pi^2\varepsilon_1^2 + 4\pi^2\varepsilon_2 - 12\pi^2\varepsilon_2 x^2)\sin(2\phi)\,\mathrm{d}t\right]. \tag{32}$$

The maximum LCE, σ_{max}, has been calculated using the above two approaches for both periodic and chaotic cases. These are reported in Figures 12 and 13. The comparison of the two algorithms seems to be quite favourable, except for one of the chaotic cases reported in Figure 13(b). Here, in contrast with a good convergence achieved using the linearization method, Iyengar's result is yet to converge even after integrating over 1000 cycles. In all these cases, the time-step, h_i, has been uniformly fixed at 0·01, Moreover, the present method is capable of extracting all the LCEs together and is computationally faster.

6.2. METHOD 2

A difficulty in implementing the above technique is the differentiation of the vector function $\mathbf{F}_i$ whose form is rather complicated. A much more elegant way to extract the LCEs is to study the eigenvalue structure of the variational equation, which, for the Duffing-Holmes oscillator, is given by equation (29). Now, let a sufficiently small interval $I = [\{x_i, \dot{x}_i\}, \{x_{i+1}, \dot{x}_{i+1}\})$ on any trajectory $X(t) = \{x(t), \dot{x}(t) \mid t \in \mathbf{R}\}$ be considered. The orientations of the two eigen-directions in equation (29) changes continuously depending on x. It is however intended here to replace these changing orientations over I by an averaged orientation. This may be achieved by replacing the time-varying coefficient of v by a constant, which in turn is obtained by minimizing the mean square error over the segment I. This leads to

$$\ddot{v} + 2\pi\varepsilon_1\dot{v} + 4\pi^2\varepsilon_2(3x_i^2 + 3x_i\Delta_i + \Delta_i^2 - 1)v = 0, \tag{33}$$

where $\Delta_i = x_{i+1} - x_i$. The two eigenvalues of the above equation are

$$
\begin{aligned}
{}^i\gamma_1 &= -\pi\varepsilon_1 + \pi\{\varepsilon_1^2 + 4\varepsilon_2(1 - 3x_i^2 + 3x_i\Delta_i + \Delta_i^2)\}^{1/2},\\
{}^i\gamma_2 &= -\pi\varepsilon_1 - \pi\{\varepsilon_1^2 + 4\varepsilon_2(1 - 3x_i^2 + 3x_i\Delta_i + \Delta_i^2)\}^{1/2}.
\end{aligned} \tag{34}
$$

Depending on x_i and Δ_i, ${}^i\gamma_{1,2}$ may be real or complex conjugates. In either case, the two local Liapunov exponents (LLEs) are given by

$$
\begin{aligned}
{}^i\sigma_{max} &= \text{Re}\,\{{}^i\gamma_1\},\\
{}^i\sigma_{min} &= \text{Re}\,\{{}^i\gamma_2\}.
\end{aligned} \tag{35}
$$

It may be mentioned that the imaginary parts of ${}^i\gamma_{1,2}$ do not contribute to the LLEs, since they give rise to fluctuating components whose time averages are strictly zero. The two LCEs are now given by

$$
\sigma_{max} = \lim_{N\to\infty} \frac{1}{N} \sum_{i=1}^{N} {}^i\sigma_{max},
$$

$$
\sigma_{min} = \lim_{N\to\infty} \frac{1}{N} \sum_{i=1}^{N} {}^i\sigma_{min}. \tag{36}
$$

It is obvious that the convergence of the LCEs calculated as above would be pretty fast as the fluctuating components are identified and removed at each step. It is interesting to

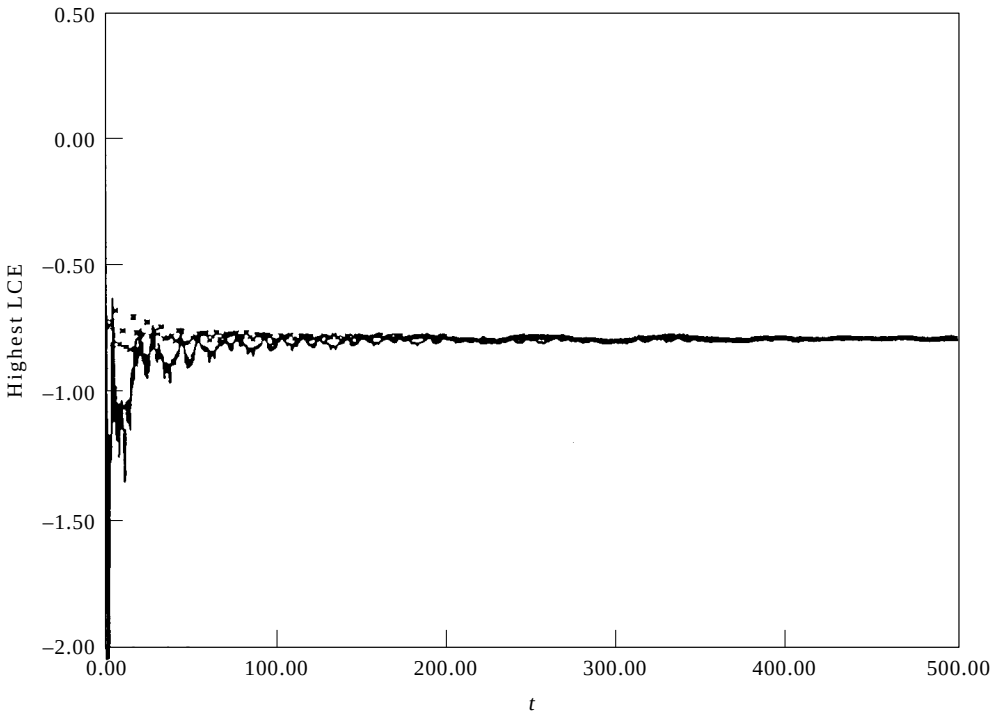

Figure 12. Highest LCE for Duffing-Holmes' oscillator via linearization (method 1) and Iyengar's schemes: one-periodic case, $\varepsilon_1 = 0{\cdot}25$, $\varepsilon_2 = 0{\cdot}5$, $\varepsilon_3 = 0{\cdot}1$. ——, Iyengar's scheme; $\times\times\times$, linearization.

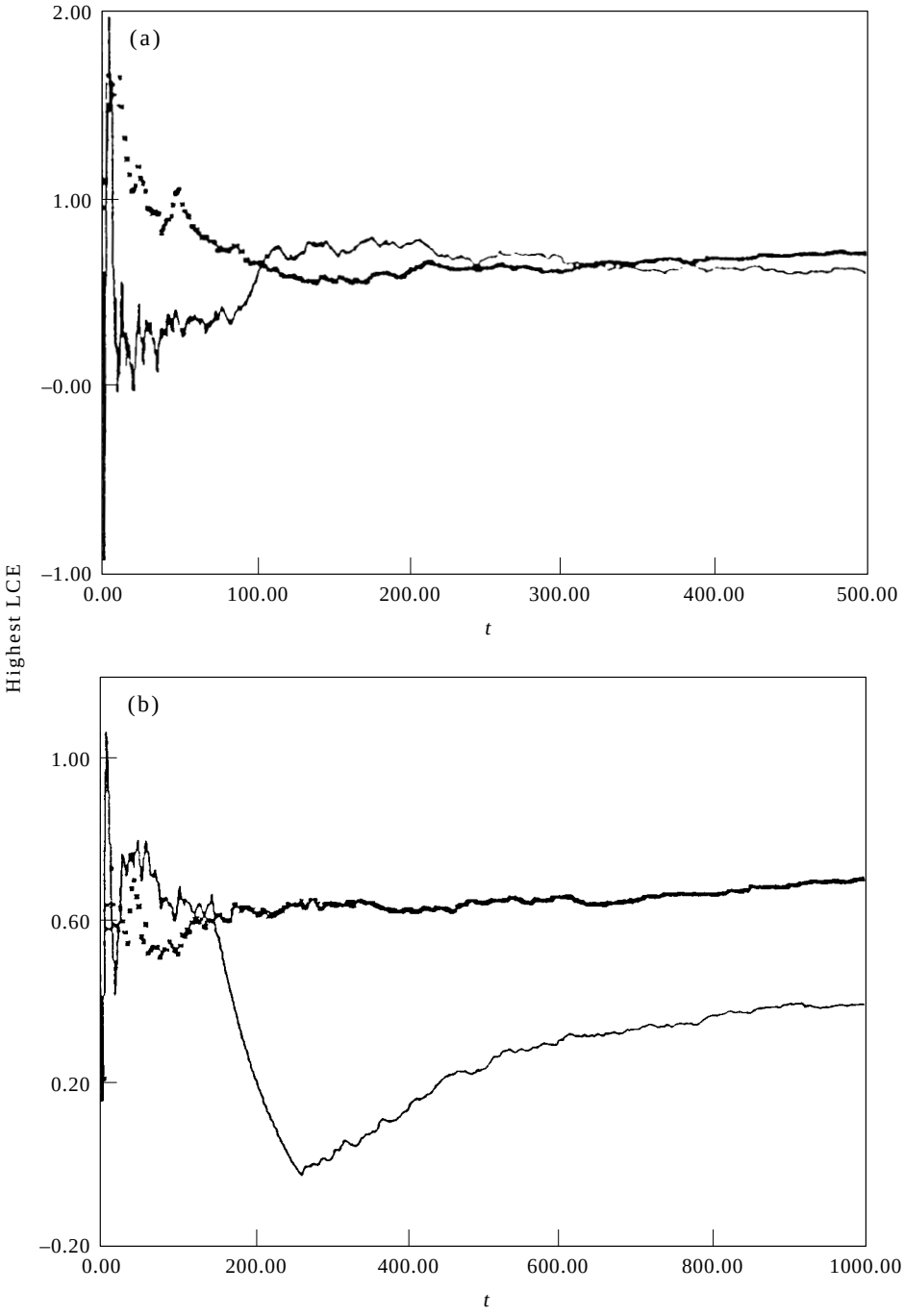

Figure 13. Highest LCE for Duffing-Holmes' oscillator via linearization (method 1) and Iyengar's schemes: chaotic cases. (a) $\varepsilon_1 = 0{\cdot}25$, $\varepsilon_2 = 0{\cdot}5$, $\varepsilon_3 = 0{\cdot}5$; (b) $\varepsilon_1 = 0{\cdot}25$, $\varepsilon_2 = 0{\cdot}3$, $\varepsilon_3 = 0{\cdot}45$. ——, Iyengar's scheme; $\times \times \times$, linearization.

observe that as long as ${}^{i}\gamma_{1,2}$ are complex conjugates (i.e., with non-zero imaginary parts), the real part remains constant at $-\pi\varepsilon_1$. Thus, the segment I can be made large so long as ${}^{i}\gamma_{1,2}$ are complex conjugates.

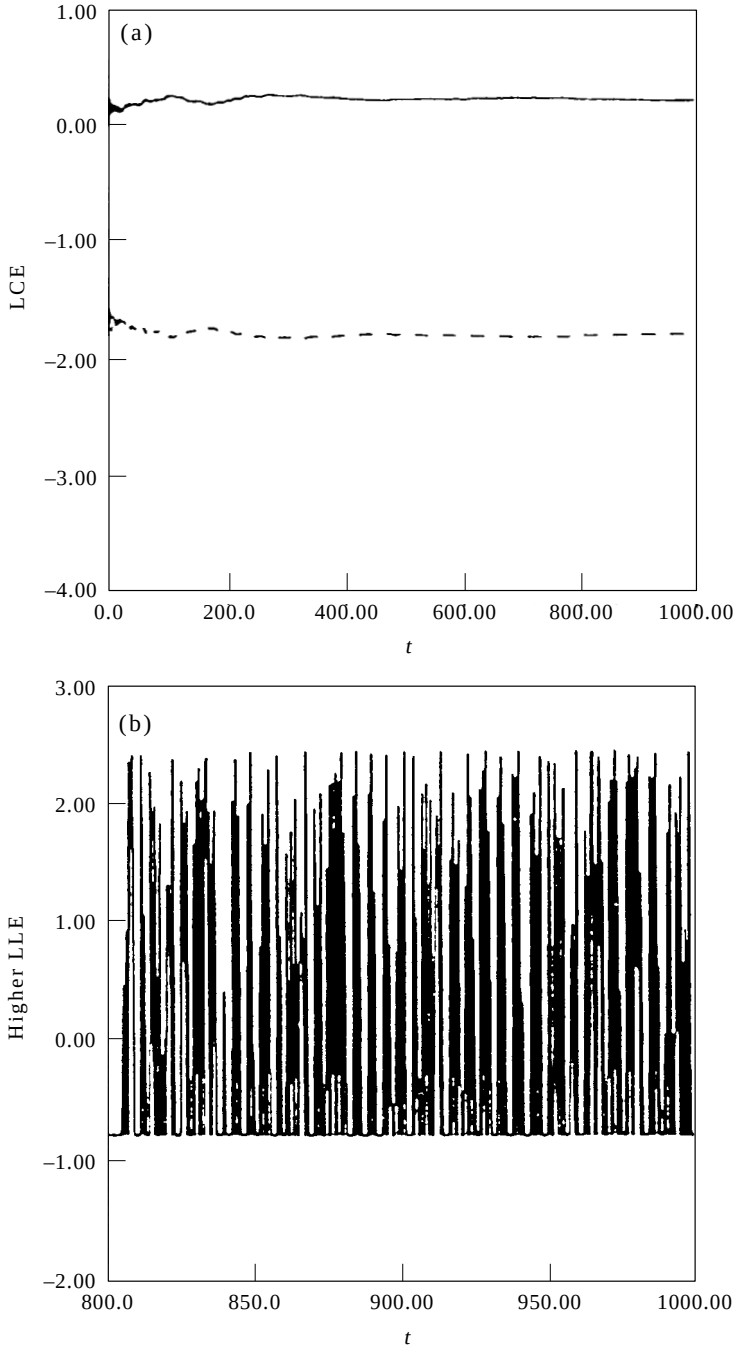

Figures 14(a)–(b)

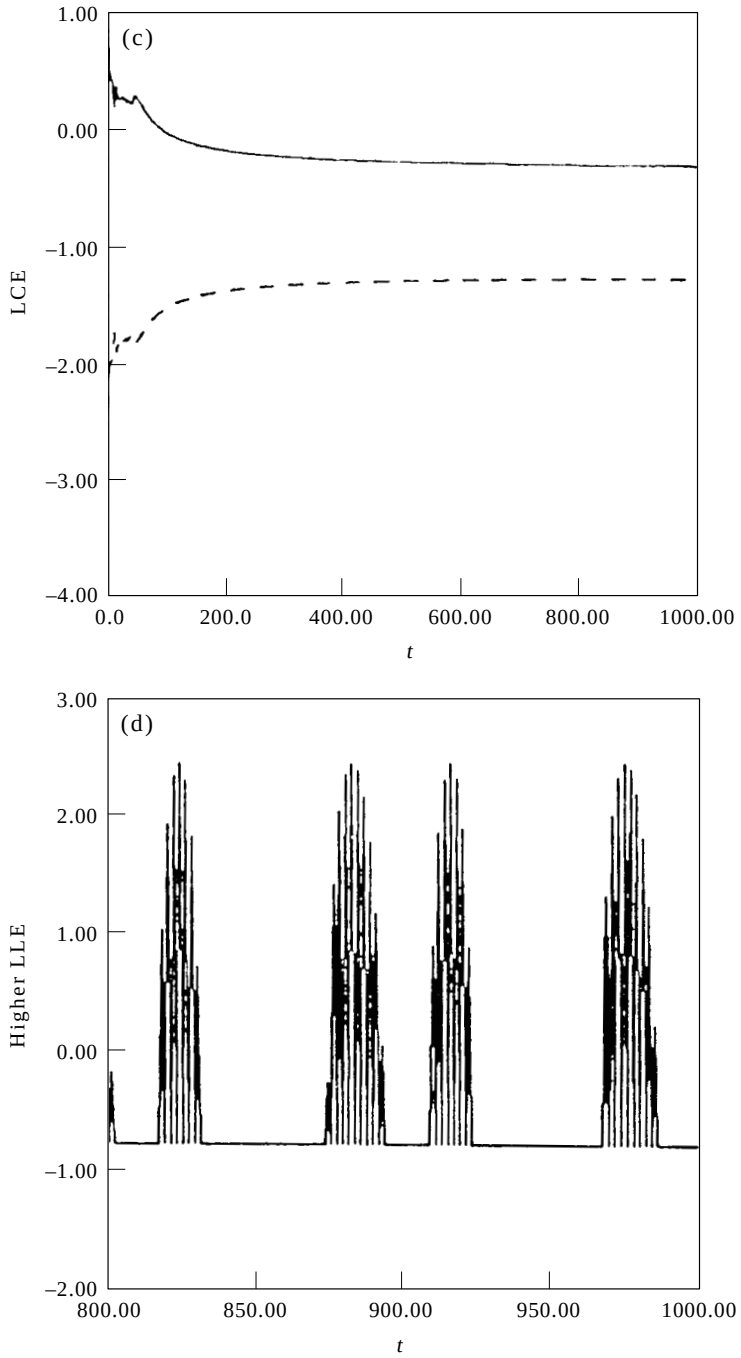

Figures 14(c)–(d)

In Figure 14, the evolutions of the two non-zero LCEs obtained using the error-minimized variational equation are shown for a few periodic and chaotic cases of the Duffing-Holmes oscillator. The corresponding evolutions of the highest LLEs are alsoreported in the same figure. From the arguments presented above, it is evident that the present technique is computationally very efficient.

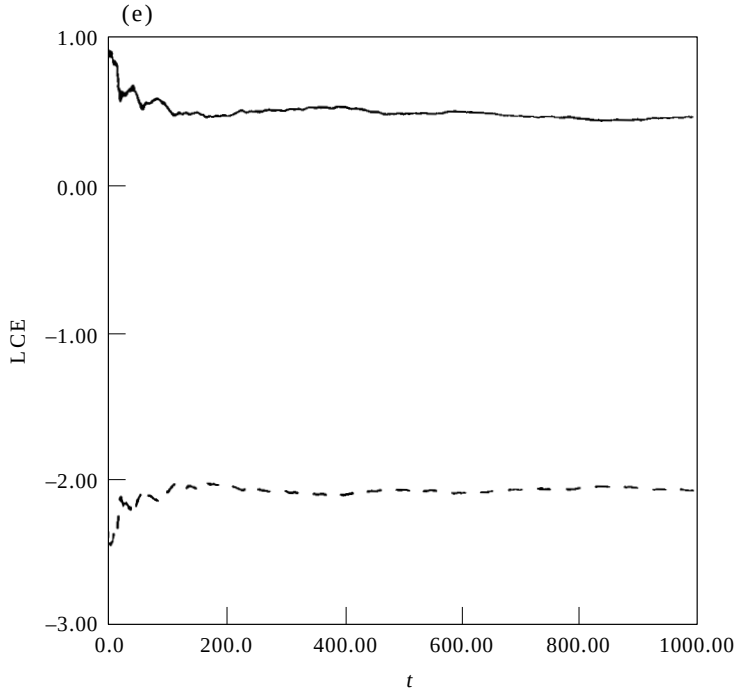

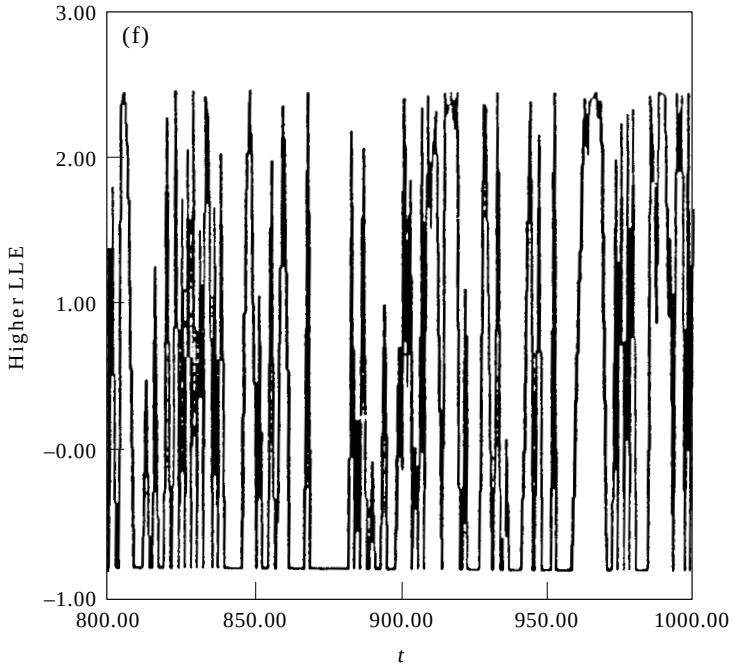

Figures 14(e)–(f)

Figure 14. (a), (b) Evolutions of the LCEs and the higher LLE of Duffing-Holmes' oscillator (method 2): $\varepsilon_1 = 0{\cdot}25$, $\varepsilon_2 = 0{\cdot}25$, $\varepsilon_3 = 0{\cdot}5$. (c), (d) $\varepsilon_1 = 0{\cdot}25$, $\varepsilon_2 = 0{\cdot}25$, $\varepsilon_3 = 0{\cdot}6$; (e), (f) $\varepsilon_1 = 0{\cdot}25$, $\varepsilon_2 = 0{\cdot}25$, $\varepsilon_3 = 0{\cdot}7$. ——, Higher LCE; – – –, lower LCE.

6.3. PROBABILITY DENSITY FUNCTIONS

It is well known that a set of chaotic trajectories starting infinitesimally close to each other separate out to finally evolve on a strange attractor which has a finite measure on a Poincaré section. In other words, if the probability density function (pdf) of the initially specified dependent variables is close to, but not exactly, a Dirac delta function, then as the trajectories evolve with time, the pdf flattens out to cover the strange attractor. The objective of this section is to make use of the map (25) for obtaining the evolution of this pdf numerically. A path integral formalism is adopted here for this purpose. A brief outline of the strategy is as follows. Let $\{x_i, \dot{x}_i\}$ be a point on the solution trajectory of equation (1) at time $t = t_i$. Given the point $\mathbf{x}_i = \{x_i, \dot{x}_i\}$, it is straightforward to obtain the point $\{x_{i+1}, \dot{x}_{i+1}\}$ at time $t = t_{i+1}$ by solving for the map (25). In other words

$$p(\mathbf{x}_{i+1} \mid \mathbf{x}_i) = \delta\{\mathbf{x}_{i+1} - \mathbf{F}_i(\mathbf{x}_i)\}, \tag{37}$$

where the vector function $\mathbf{F}_i$ is given by

$$\mathbf{F}_i = \{F_{1i} \quad F_{2i}\}, \tag{38}$$

and δ stands for the Dirac delta function. Now it is noted that the following relation is an identity

$$p(\mathbf{x}_{i+1}) = \int_{\mathbf{x}_i} \int p(\mathbf{x}_{i+1} \mid \mathbf{x}_i) p(\mathbf{x}_i)\, \mathrm{d}\mathbf{x}_i. \tag{39}$$

Substitution of equation (37) in the above equation leads to

$$p(\mathbf{x}_{i+1}) = p\{\mathbf{F}_i^{-1}(\mathbf{x}_{i+1})\}. \tag{40}$$

However, in the above algorithm, $\mathbf{F}_i$ is a point-to-point mapping. Therefore, in a computer simulation, a point once visited is almost surely never visited again due to the limitations of floating point representation of numbers. To overcome this difficulty, it would be convenient to divide the continuum of the phase space into a countable number of rectangular cells. Each cell is assumed to be represented by its centre point and this representative point is assumed to be visited by an ensemble of trajectories as many times as the corresponding cell is visited. Thus, depending on the cell size, it is possible to obtain a unique cell map from the point-to-point map (25). Let the cell map be given by

$$s_{i+1} = \mathbf{S}_i(s_i), \tag{41}$$

where s_i, $i = 1, 2, \ldots$ are a set of regular cells [13], such that $\cup_i s_i$ is a cover for the attractor in a Poincaré section. The set $\{\cup_i s_i\}^c$ is replaced by a single sink cell, where the superscript 'c' stands for complementation. Since the inverse $\mathbf{F}_i^{-1}$ exists for sufficiently small $[t_i, t_{i+1})$ and each cell s_i is denoted by a unique point, it follows that the inverse $\mathbf{S}_i^{-1}$ also exists. Therefore, equations (38) through (41) may be easily reformulated with reference to the cell state space. Thus,

$$p(s_{i+1} \mid s_i) = \delta\{s_{i=1} - \mathbf{S}_i(s_i)\} \tag{42}$$

and

$$p(s_{i+1}) = p\{\mathbf{S}_i^{-1}(s_{i+1})\}. \tag{43}$$

To implement the above algorithm, an ensemble of initial trajectories, each starting from the centre of a cell, is chosen. In order to find out all the attractors that may be present

in the phase space, it is appropriate to start with non-zero initial probabilities for each of the cells. A convenient choice is a uniform pdf, i.e., $p(s_i) = 1/N$, where N stands for the number of regular cells. The evolution of the pdf may now be numerically computed using equations (42) and (43). It may be noted that at any time, $t = t_j$, a cell s_j can either have a zero probability or a probability in terms of multiples of $1/N$. Therefore it is essential to choose a sufficiently high N in order to obtain a smooth pdf.

Before applying the above algorithm to non-linear ODEs, it would be useful to verify the approach for the logistic map, for which quite a number of results are already available in the literature. This map is given by

$$x_{i+1} = \mu x_i(1 - x_i), \tag{44}$$

where, $0 \leqslant x_i \leqslant 1$ for all i. The closed interval [0, 1] is now divided into 5000 cells of the same size. Similarly, a set of 5000 initial conditions, each starting from the middle of the corresponding cell, has been chosen. In Figure 15, the resulting pdf at the 1000-th iteration of equation (44) have been shown for three different chaotic cases corresponding to $\mu = 3{\cdot}8$, $3{\cdot}825$ and $4{\cdot}0$. A visual comparison of these results with those obtained by Shaw [14] using an iterative scheme shows very good agreement. It may however be mentioned that for the logistic map, the trajectories are ergodic and therefore a stationary pdf exists, which can be computed using only a single trajectory instead of an ensemble.

Next, the algorithm is applied to the Duffing-Holmes oscillator. When the oscillator is in the chaotic regime, the solution evolves within the strange attractor. First, the strange attractor is shown in Figure 16(a). The corresponding pdf at $t = 100$ s is shown in Figure 16(b). Here an ensemble of 2500 trajectories have been used and consequently the phase plane has been divided into 50×50 rectangular cells of the same size. From this figure, the non-stationary nature of the PDF is evident.

7. DISCUSSION AND CONCLUSIONS

The aim of this paper has been to explore the new phase space linearization method in order to verify the universality of the method as applied to harmonically forced non-linear oscillators. In particular, it has been shown that the method is capable of simulating a wide variety of orbits, such as period-doubled orbits, quasi-periodic orbits and even chaotic orbits, which are distinctive to non-linear oscillators. It has also been demonstrated that a rich repertoire of information may be obtained by inspecting the local eigenvalue structure of the equivalent linear equations, each valid over small segments of the orbit in the relevant phase space. Thus, it has been possible to develop a strategy for constructing the stable and unstable invariant manifolds which are normally hyperbolic to the unstable limit cycle of the Duffing-Holmes oscillator. Since the stable manifold is the same as the separatrix, that delimits the basins of attraction of the pair of stable limit cycles. Such a strategy serves the additional purpose of structuring the initial condition plane without the necessity of performing an elaborate and time-consuming numerical integration. Moreover, an inspection of eigenvalues leads to a very efficient algorithm to construct the small one-periodic orbits, in addition to the unstable limit cycle of the Duffing-Holmes oscillator. This in turn permits an investigation of near-tangency of the stable and unstable one-periodic orbits, leading to an approximate boundary in the parameter space, beyond which chaotic diffusion is a distinct possibility. Next it is shown that the concept of piecewise linearization may be used for an accurate determination of Fourier spectra of the response process. It has been pointed out that the PSL method may be applied to reduce the flow of a non-linear oscillator either to a non-linear map or to an equivalent linear flow over small segments of the relevant orbit. These aspects have been exploited to arrive

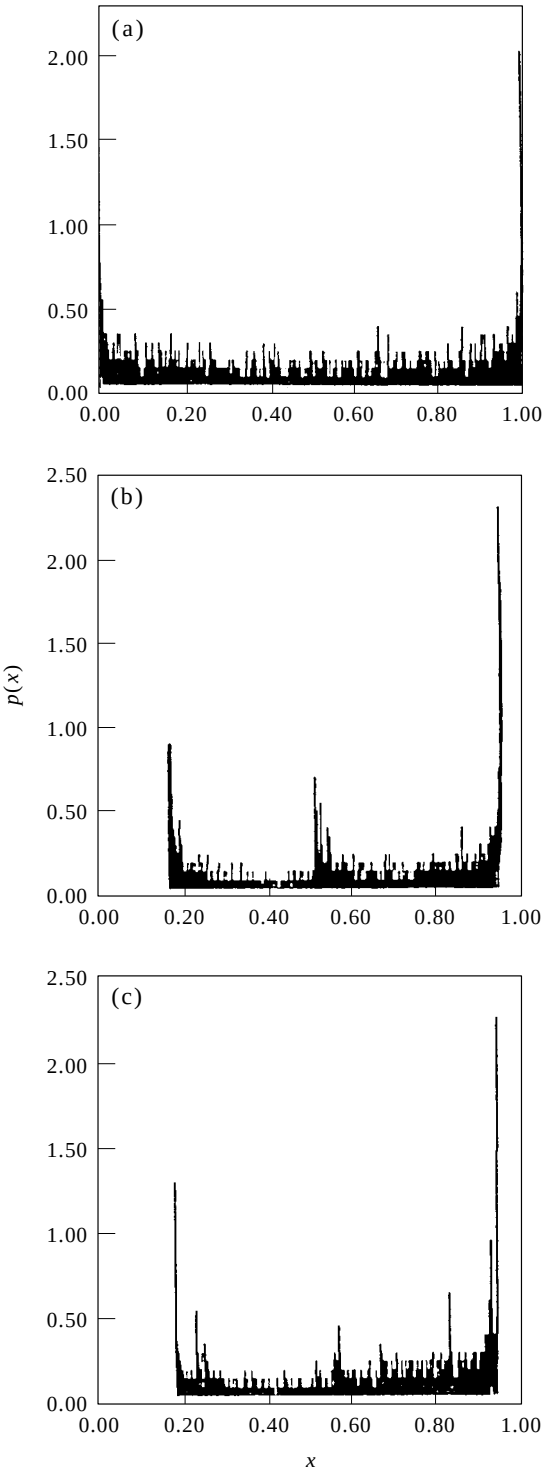

Figure 15. PDF for the logistic map: (a) $\mu = 3{\cdot}8$, (b) $\mu = 3{\cdot}825$; (c) $\mu = 4{\cdot}0$.

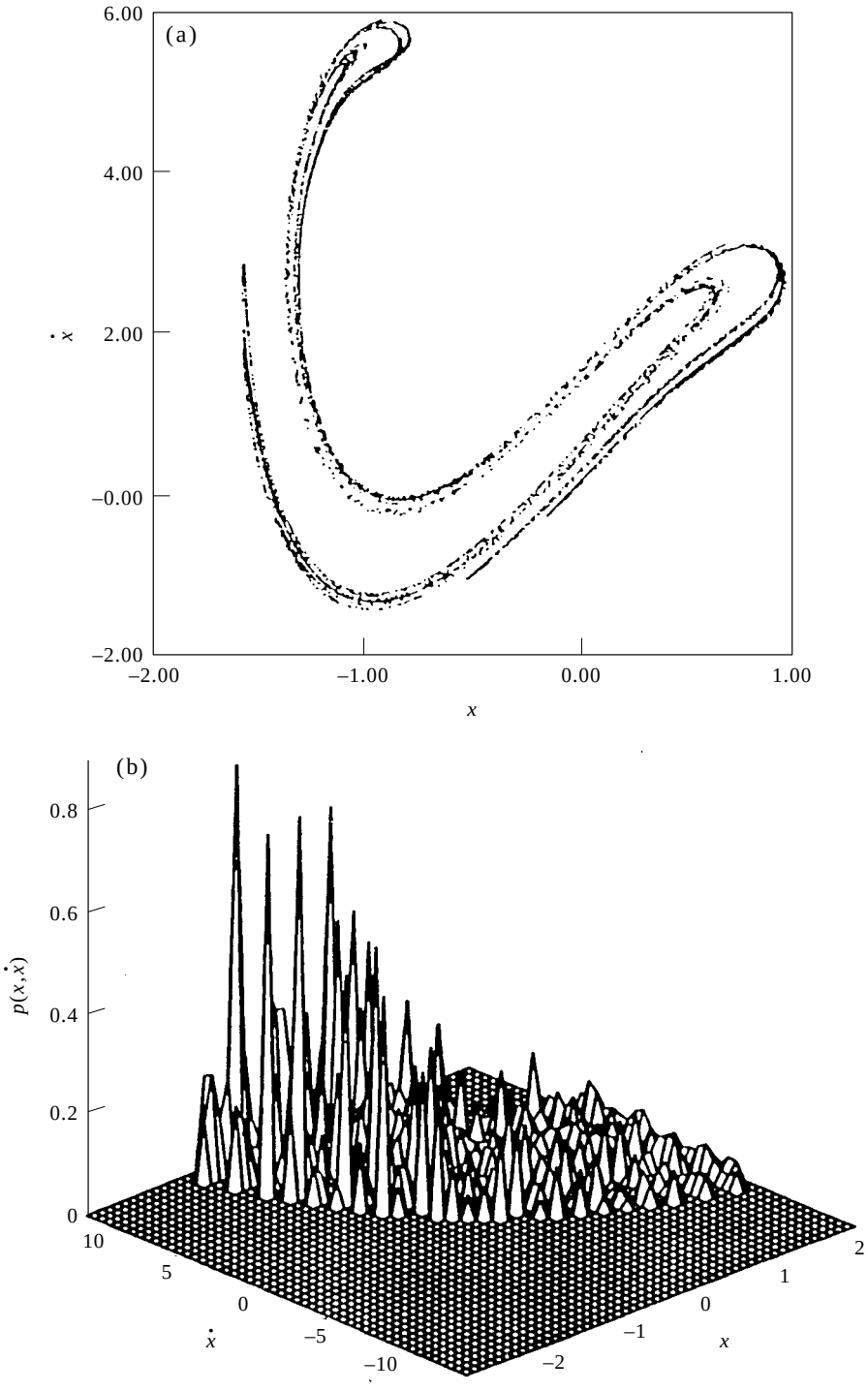

Figure 16. (a) Chaotic case of Duffing-Holmes' oscillator: strange attractor on a Poincaré section, $\varepsilon_1 = 0{\cdot}25$, $\varepsilon_2 = 0{\cdot}3$, $\varepsilon_3 = 0{\cdot}45$. (b) PDF of Duffing-Holmes' oscillator for the chaotic case.

at two different methods for calculating all the Liapunov characteristic exponents. Finally, the method has been made use of in numerically determining the probability density function of an ensemble of chaotic trajectories.

Here it needs to be mentioned that the arguments presented for determining the near-tangency of stable and unstable one-periodic orbits of the Duffing-Holmes oscillator are rather heuristic and lack sound analytical footing. Thus, a better way of performing such an analysis would be to choose a Poincaré section and then derive a Melnikov-type of function for the distance between the stable and unstable orbits by making use of the new linearization scheme. However, such a rigorous analysis poses several difficulties and it is not pursued here. The boundary for the near-tangency of the stable and unstable orbits should therefore be interpreted as approximate.

The proposed PSL technique, as of now, lacks a sound mathematical footing. It appears that the error minimization is not the only way to obtain the conditionally linear equations. Thus, efforts to find out these equivalent linear equations by other means should be made. Once various methods for constructing these equations are established and mathematically validated, the interrelationship between these methods needs to be found out. This will shed new light on non-linear response characteristics. Here it may be pointed out that the PSL scheme should be readily extendible to higher dimensional non-linear oscillators, wherein solutions of a set of non-linear algebraic equations at each step would be required to find out the unknown increments of various dependent coordinates. Finally, it is noted that extension of the concept of PSL to non-linear random vibration problems forms another interesting piece of unaccomplished task. It is hoped that the work reported here would invite the attention of researchers in these directions.

REFERENCES

1. R. N. Iyengar and D. Roy 1998 *Journal of Sound and Vibration* **211**, 843–875. New approaches for the study of non-linear oscillators.
2. P. E. Kloeden and J. Lorenz 1986 *SIAM Journal of Numerical Analysis* **23**, 986–995. Stable attracting sets in dynamical systems and in their one-step discretisation.
3. E. N. Lorenz 1989 *Physica D* **35**, 299–317. Computational chaos: a prelude to computational instability.
4. R. M. Corless, C. Essex and M. A. H. Nerenberg 1991 *Physics Letters A* **157**, 27–36. Numerical methods can suppress chaos.
5. S. T. Fryska and M. A. Zohdy 1992 *Physics Letters A* **166**, 340–346. Computer dynamics and shadowing of chaotic orbits.
6. M. Kleczka, W. Kleczka and E. Kreuzer 1990 in *Continuation and Bifurcations*: *Numerical Techniques and Applications* (D. Roose *et al*., editors). Dordrecht: Kluwer Academic Publishers. A combined numerical and analytical approach.
7. W. Kleczka, E. Kreuzer and C. Wilmers 1991 *International Series Num. Math.* **97**, 199–203. Combined analytical-numerical analysis of nonlinear dynamical systems.
8. J. Guckenheimer and P. Holmes 1983 *Nonlinear Oscillations*, *Dynamical Systems*, *and Bifurcations of Vector Fields*. Springer-Verlag.
9. M. W. Hirsch, C. C. Pugh and M. Shub 1977 *Invariant Manifolds*. Springer Lecture Notes in Mathematics, Vol. 583. Berlin: Springer-Verlag.
10. E. H. Dowell and C. Pezeshki 1988 *Journal of Sound and Vibration* **121**, 195–200. On necessary and sufficient conditions for chaos to occur in Duffing's equation: an heuristic approach.
11. W. Szemplinska-Stupnicka and J. Rudowski 1992 *Journal of Sound and Vibration* **152**, 57–72. Local methods in predicting occurrence of chaos in two-well potential systems: superharmonic frequency regions.
12. R. N. Iyengar 1993 *ZAMM* **73**, T46–T53. Chaotic behaviour in nonlinear oscillators.
13. C. S. Hsu 1980 *Journal of Applied Mechanics* **47**, 931–939. A theory of cell-to-cell mapping dynamical systems.
14. A. J. Lichtenberg and M. A. Lieberman 1983 *Regular and Stachastic Motion*. Berlin: Springer-Verlag.